



**HAL**  
open science

## Dynamical phase coexistence in the Fredrickson–Andersen model

Robert L. Jack, Takahiro Nemoto, Vivien Lecomte

► **To cite this version:**

Robert L. Jack, Takahiro Nemoto, Vivien Lecomte. Dynamical phase coexistence in the Fredrickson–Andersen model. *Journal of Statistical Mechanics: Theory and Experiment*, 2020, 2020 (5), pp.053204. 10.1088/1742-5468/ab7af6 . hal-03093421

**HAL Id: hal-03093421**

**<https://hal.science/hal-03093421>**

Submitted on 3 Jan 2021

**HAL** is a multi-disciplinary open access archive for the deposit and dissemination of scientific research documents, whether they are published or not. The documents may come from teaching and research institutions in France or abroad, or from public or private research centers.

L'archive ouverte pluridisciplinaire **HAL**, est destinée au dépôt et à la diffusion de documents scientifiques de niveau recherche, publiés ou non, émanant des établissements d'enseignement et de recherche français ou étrangers, des laboratoires publics ou privés.

# Dynamical phase coexistence in the Fredrickson-Andersen model

Robert L Jack<sup>1,2</sup>, Takahiro Nemoto<sup>3,4</sup>, Vivien Lecomte<sup>5</sup>

<sup>1</sup> DAMTP, Centre for Mathematical Sciences, Wilberforce Road, Cambridge CB3 0WA, United Kingdom

<sup>2</sup> Department of Chemistry, Lensfield Road, Cambridge CB2 1EW, United Kingdom

<sup>3</sup> Philippe Meyer Institute for Theoretical Physics, Physics Department, École Normale Supérieure & PSL Research University, 24 rue Lhomond, 75231 Paris Cedex 05, France

<sup>4</sup> Mathematical Modelling of Infectious Diseases Unit, Institut Pasteur, 25-28 Rue du Docteur Roux, 75015 Paris, France.

<sup>5</sup> LIPhy, Université Grenoble Alpes & CNRS, F-38042 Grenoble, France

**Abstract.** We analyse a first-order dynamical phase transition that takes place in the Fredrickson–Andersen (FA) model. We construct a two-dimensional spin system whose thermodynamic properties reproduce the dynamical large deviations of the FA model and we analyse this system numerically, comparing our results with finite-size scaling theory. This allows us to rationalise recent results for the FA model, including the exponential divergence of its susceptibility at phase coexistence. We also discuss a simple interfacial model that reproduces quantitatively the behaviour of the FA model at coexistence.

## 1. Introduction

Large deviation theory is an increasingly useful tool for understanding dynamical fluctuations in statistical mechanics [1, 2, 3, 4, 5, 6]. For example, by analysis of probability distributions of time-averaged quantities, one gains understanding of entropy production and dissipation [7, 8, 9], transport phenomena [10, 2, 11, 12, 13], and metastability in glassy systems [14, 15, 16, 17]. The tails of these probability distributions can have characteristic forms, which are related to a particular type of dynamical phase transition [10, 14, 15]. These are analogous to thermodynamic phase transitions, in that one analyses ensembles of dynamical trajectories in a manner that is exactly analogous to the classical analysis of thermodynamic ensembles. While the principles of thermodynamics are restricted to static and quasistatic phenomena, applications of large deviation theory to trajectories of these systems can be viewed as an extension of the thermodynamic formalism to the analysis of dynamical phenomena [18, 19, 3, 4].

The analogy between static and dynamical phase transitions means that methods from thermodynamics can often be generalised, in order to study dynamical transitions.

For example, the dynamical analogue of the free energy can be obtained as the solution to an eigenvalue problem [2, 5, 20], just as the thermodynamic free energy can be obtained as the largest eigenvalue of a transfer matrix. The numerical method of transition path sampling [21] generalises Monte Carlo sampling techniques from static configurations to dynamical trajectories [19, 22]. However, there are also methods that harness directly the dynamical aspects of trajectory ensembles, including cloning (population dynamics) methods for numerics [23, 24], and control-theoretic approaches that aim to describe dynamical rare events by constructing controlled processes where these events become typical [16, 25, 26].

In a recent paper [27], we analysed the finite-size scaling of a first-order dynamical phase transition in the Fredrickson–Andersen (FA) model [28]. This simple model describes glassy systems [29, 30] and has been studied extensively in that context. Its dynamical phase transition is also amenable to analytic and numerical studies [14, 4, 17, 31, 32, 27, 33]. In [27], we used a cloning method to demonstrate an exponential divergence of the susceptibility with system size, and we explained this behaviour analytically. This exponential divergence stands in contrast to the usual finite-size scaling behaviour at *thermodynamic* first-order transitions, where one observes a power-law divergence with system size. The different scaling behaviour arises from the way in which the thermodynamic limit is taken: when considering the distribution of a time-averaged quantity, the large-time limit is taken before the large system-size limit, requiring the analysis of two distinct scaling variables. In this work, we analyse in more detail the connection between finite-size scaling analyses for thermodynamic and dynamical phase transitions.

Our results consist of two main parts. First, we define a two-dimensional ( $2d$ ) spin model whose behaviour can be related directly to trajectories of the one-dimensional FA model. This spin model has a thermodynamic phase transition that reproduces all aspects of the FA dynamical phase transition. We present numerical results that illustrate this fact. In particular, we show that by considering systems on lattices with different aspect ratios, we can capture the differences in finite-size scaling behaviour between the usual thermodynamic setting (aspect ratio close to unity) and the dynamical one (very large aspect ratio). This observation is related to a theoretical analysis of thermodynamic finite-size scaling by Privman and Fisher [34] and Borgs and Kotecký [35, 36]. In the second part of this paper, we revisit the analytical results of [27], which concern an interfacial model that captures quantitatively the finite-size scaling behaviour of the FA model. We show how some of the results can be simplified by taking a suitable limit, and we discuss the physical interpretation of this model in more detail. We explain that our results for finite-size scaling behaviour are generic for first-order dynamical transitions.

The paper is structured as follows: Sec. 2 reviews the behaviour of the FA model and its phase transition. Sec. 3 introduces the  $2d$  spin model and Sec. 4 has the results for this model. Sec. 5 analyses the interfacial model. Our conclusions are summarised in Sec. 6.

## 2. Large deviations in the FA model

This Section recalls the definition of the FA model [28] and summarises some previous results for its dynamical phase transition [14, 4].

### 2.1. Model

The (one-dimensional) FA model is a Markov chain in continuous time. It consists of  $L$  spins on a  $1d$  lattice with periodic boundaries, the  $i$ th spin is  $n_i \in \{0, 1\}$ . Let  $\mathbf{n} = (n_1, n_2, \dots, n_L)$ . Spin  $i$  can flip (that is, change its state) only if a constraint function  $C_i(\mathbf{n})$  is non-zero. In this work we take  $C_i(\mathbf{n}) = n_{i+1} + n_{i-1} - n_{i+1}n_{i-1}$  so that  $C_i \in \{0, 1\}$ . We also introduce a numerical parameter  $c \in (0, 1)$ . Then, spins with  $n_i = 0$  flip to  $n_i = 1$  with rate  $cC_i(\mathbf{n})$ ; spins with  $n_i = 1$  flip to  $n_i = 0$  with rate  $(1-c)C_i(\mathbf{n})$ . We note in passing that some other studies take instead  $C_i = n_{i-1} + n_{i+1}$  which leads to very similar behaviour. Our choice in this work is convenient because it simplifies the spin model defined in Sec. 3.2 below. Note also that no spin flips can ever cause the system to enter or leave the state  $\mathbf{0} = (0, 0, \dots, 0)$ . Hence, in order to ensure that the dynamics is irreducible, we define its configuration space as the set of all spin configurations except for  $\mathbf{0}$ .

The FA model respects detailed balance with respect to a steady-state (equilibrium) probability distribution where all spins are independent, and  $\langle n_i \rangle_0 = c$ . That is, in the equilibrium state one has

$$p(\mathbf{n}_t) \propto \exp\left(-\frac{h}{T} \sum_i n_{i,t}\right), \quad (1)$$

where  $(h/T) = \log[(1-c)/c]$ ; we identify  $T$  as the temperature. [To be precise, (1) is applicable only if  $\mathbf{n}_t \neq \mathbf{0}$ .]

### 2.2. Large deviations

We briefly describe the large-deviation formalism for the dynamical activity. For full details see [4], general discussions of large deviation theory can be found in [1, 5]. Consider a dynamical trajectory where the time  $t$  runs from 0 to  $\tau$ . Let  $K(\tau)$  be the total number of spin flip events that occur during this time interval. The average  $\langle K(\tau) \rangle_0 = \tau \bar{k} L$  with  $\bar{k} = 2c^2(2-c)(1-c)$ . Since the model is a finite irreducible Markov chain, the probability distribution for  $K(\tau)$  obeys an large-deviation principle (LDP) [1, 37, 3, 4, 5]:

$$\text{Prob}[K(\tau) \approx \tau k L] \asymp \exp[-\tau I_L(k)], \quad (2)$$

where  $I_L$  is the rate function, which is analytic and strictly convex. Note that the speed of this LDP is  $\tau$  and that the system size  $L$  is fixed as  $\tau \rightarrow \infty$ .

Large deviation theory describes rare events where  $K(\tau)$  takes a value far from its mean. To analyse these rare events it is convenient to introduce a biasing field  $s$  and to

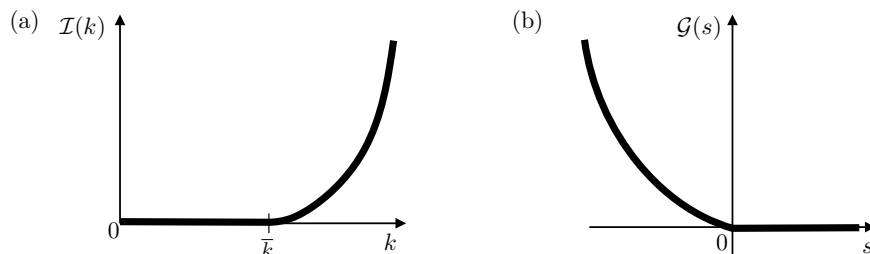


**Figure 1.** Sketches of  $\mathcal{I}(k)$  and  $\mathcal{G}(s)$  for the FA model, based on the theory of [14, 4]. The first derivative of  $\mathcal{I}$  is continuous at  $k = \bar{k}$  but the second derivative is discontinuous there. (Note  $\mathcal{I}'(k) = 0$  for  $k \leq \bar{k}$ .) The first derivative of  $\mathcal{G}$  is discontinuous at  $s = 0$  (with  $\mathcal{G}'(s) = 0$  for  $s > 0$ ).

define the scaled cumulant generating function (SCGF)

$$G_{L,\tau}(s) = \frac{1}{\tau} \log \langle e^{-sK(\tau)} \rangle_0. \quad (3)$$

The angle brackets with subscript 0 indicate a steady-state (equilibrium) average over trajectories running between time 0 and  $\tau$ . Also define

$$G_L(s) = \lim_{\tau \rightarrow \infty} G_{L,\tau}(s). \quad (4)$$

Then the rate function can be obtained as  $I_L(k) = \sup_s [-skL - G_L(s)]$ . Also, the rare events of interest can be analysed by considering biased ensembles of trajectories in which the average of any (trajectory-dependent) observable  $O$  is

$$\langle O \rangle_s = \frac{\langle O e^{-sK} \rangle_0}{\langle e^{-sK} \rangle_0}. \quad (5)$$

Results for equivalence of ensembles [3, 38] show that for a large class of observables  $O$ , the biased average  $\langle O \rangle_s$  converges (as  $\tau \rightarrow \infty$ ) to a conditional average of  $O$  in the original (unbiased) process, where  $K(\tau)$  is constrained to take a particular value. This constraint is  $K(\tau) = \tau L \cdot k_L(s)$  with  $k_L(s) = -G'_L(s)/L$ .

Let  $p_{L,\tau}(K)$  be the probability to observe exactly  $K$  spin flips and let  $\rho_{L,\tau}(k) = \tau L \cdot p_{L,\tau}(\tau L k)$  be an associated probability density for  $k = K/(L\tau)$ . The rate function that appears in (2) may be obtained as

$$I_L(k) = \lim_{\tau \rightarrow \infty} \frac{-1}{\tau} \log \rho_{L,\tau}(k). \quad (6)$$

### 2.3. Dynamical phase transition

Since the FA model is an irreducible finite-state Markov chain, the Perron–Frobenius theorem establishes that  $I_L(k)$  and  $G_L(s)$  are analytic and (strictly) convex [3, 5, 20]. To reveal the dynamical phase transition that occurs in the model, one defines a bulk free energy density and a scaled rate function

$$\mathcal{G}(s) = \lim_{L \rightarrow \infty} \frac{1}{L} G_L(s), \quad \mathcal{I}(k) = \lim_{L \rightarrow \infty} \frac{1}{L} I_L(k). \quad (7)$$

The form of these limiting functions  $\mathcal{G}, \mathcal{I}$  is not constrained by the Perron–Frobenius theorem, see [39] for a discussion. In the FA model, these functions have singularities, as sketched in Fig. 1. Note in particular that  $\mathcal{I}(k) = 0$  for  $0 < k \leq \bar{k}$  and  $\mathcal{G}(s) = 0$  for all  $s \geq 0$  [14, 4, 31]. In the analogy with equilibrium statistical mechanics, this corresponds to a first-order phase transition.

### 3. From the 1d FA model to a 2d spin system

In this Section we formulate a discrete-time FA (dFA) model with synchronous spin updates. The time between updates is  $\delta t$  and taking  $\delta t \rightarrow 0$  recovers the (original) FA model. We also explain how trajectories of this model can be mapped onto configurations of a 2d spin system. Hence dynamical large deviations of the dFA and FA models can be analysed by computing thermodynamic properties of this 2d spin system.

#### 3.1. Discrete-time FA model

The configuration of the discrete-time FA model at time  $t$  is  $\mathbf{n}_t$ . The configuration at time  $t + \delta t$  is generated by the following (stochastic) procedure. We first construct a set of random variables  $\mathbf{m}_t = (m_{1,t}, m_{2,t}, \dots, m_{L,t})$  with  $m_{i,t} \in \{0, 1\}$ . The idea is that if  $m_i = 0$  then spin  $n_i$  cannot change its state between times  $t$  and  $t + \delta t$ . The  $m$ -variables are chosen from a distribution (independent of  $t$  and  $\mathbf{n}$ ):

$$p(\mathbf{m}) = \frac{1}{z(\gamma)} \exp\left(-\gamma \sum_i m_i\right) \prod_i \tilde{C}_i(m_i, m_{i+1}) \quad (8)$$

where  $\gamma$  is a parameter and  $z(\gamma)$  is a normalisation constant (see below); also  $\tilde{C}(m_i, m_{i+1}) = 1 - m_i m_{i+1}$ , which enforces that adjacent sites cannot both have  $m = 1$ .

Given the vector  $\mathbf{m}_t$ , the spin variables  $n_{i,t+\delta t}$  are then generated independently, by the following rule:

$$\begin{aligned} \text{If } C_i(\mathbf{n}_t) = 0 \text{ or } m_i = 0 \text{ then } n_{i,t+\delta t} &= n_{i,t} \\ \text{otherwise } n_{i,t+\delta t} &= 1, 0 \text{ with probs } c, (1 - c) \text{ respectively} \end{aligned} \quad (9)$$

The dependence on  $m_i$  together with the constraint  $\tilde{C}$  means that if spin  $n_i$  flips on a given time step then neither spin  $n_{i-1}$  nor spin  $n_{i+1}$  can flip. Hence, if spin  $i$  flips then  $C_i(\mathbf{n}_t) = 1 = C_i(\mathbf{n}_{t+\delta t})$ . This last property can be used to show that the update rule respects detailed balance with respect to the same steady state distribution as the FA model.

Positive values of the parameter  $\gamma$  increase the probability that  $m_i = 0$  and reduce the number of sites at which the  $n$ -spins can flip. It is easily seen that  $z(\gamma)$  is the partition function for a gas of 1d hard rods with length 2 and chemical potential  $-\gamma T$ , on a lattice of size  $L$ . For large  $\gamma$ , the typical number of spins that are able to flip in a single update is small, and  $z$  is close to the partition function for an ideal gas. If one takes

$$\gamma = -\log \frac{\delta t}{1 - \delta t} \quad (10)$$

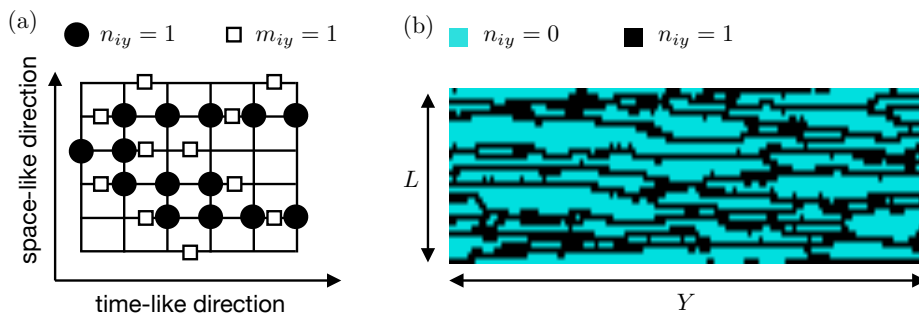


**Figure 2.** Illustration of the  $2d$  spin model. (a) The model is defined on a square lattice. It is anisotropic, with a space-like direction corresponding to the  $1d$  lattice of the analogous FA model and a time-like direction that corresponds to the time axis for the FA model. The vertices (sites) of the square lattice are occupied by  $n$ -variables, and sites with  $n_{iy} = 1$  are indicated with filled circles. All other vertices have  $n_{iy} = 0$ . The horizontal (time-like) bonds are occupied by  $m$ -variables: bonds with  $m_{iy} = 1$  are indicated by open squares. (b) A representative configuration of this model obtained by Monte Carlo sampling with  $c = 0.38$ ,  $\gamma = 0$ , and  $(L, Y) = (32, 128)$ . Only the  $n$ -variables are shown. This resembles a typical trajectory of the continuous-time FA model [29].

and  $\delta t \rightarrow 0$  then the dFA model reproduces the behaviour of the FA model.

### 3.2. Corresponding spin model

We now define the  $2d$  spin model whose configurations correspond to trajectories of the dFA model. For a trajectory of length  $\tau$ , let  $Y = \tau/\delta t$  be the number of time steps in the discrete-time FA model. The  $2d$  model is defined on a decorated lattice, illustrated in Fig. 2(a). The lattice contains  $(L \times Y)$  primary sites, which are associated with variables  $n_{i,y} \in \{0, 1\}$  with  $i = 1, 2, \dots, L$  and  $y = 1, 2, \dots, Y$ . The index  $y$  indicates the position along the *time-like* axis (horizontal in Fig. 2) and the index  $i$  is the position on the space-like axis. The  $m$ -variables of the dFA model are defined on the time-like bonds of the lattice. They are  $m_{i,y} \in \{0, 1\}$  with  $i = 1, 2, \dots, L$  and  $y = 1, 2, \dots, (Y - 1)$ .

The configurations of this model are in exact correspondence with trajectories of the discrete-time FA model, as long as one enforces the following constraints: the FA configuration  $\mathbf{0}$  is not allowed so  $\sum_i n_{i,y} > 0$  for all  $y$ ; the  $m$ -variables on spatially adjacent sites cannot both be in state 1 so  $m_{i,y} m_{i+1,y} = 0$  for all  $y$ ; an FA spin can only flip if  $m_{i,t} = 1$  and  $C_i(\mathbf{n}_t) = 1$ , so  $\delta(n_{i,y} - n_{i,y+1}) + m_{it}(n_{i-1,t} + n_{i+1,t}) > 0$  where  $\delta(x) = 1$  if  $x = 0$  and  $\delta(x) = 0$  otherwise. These constraints define the configuration space of the spin model.

We now define an energy function so that the Boltzmann–Gibbs distribution of the  $2d$  model at temperature  $T = 1$  corresponds to the steady-state trajectory measure for the discrete-time FA model. This energy is

$$E_0 = -\log \rho_0(\mathbf{n}_1) - \sum_{y=1}^{Y-1} \log P(\mathbf{n}_{y+1} | \mathbf{n}_y), \quad (11)$$

where  $\rho_0(\mathbf{n})$  is the steady-state probability of configuration  $\mathbf{n}$  in the FA model, and  $P(\mathbf{n}|\mathbf{n}')$  is the transition probability for the discrete-time dynamics. The result is

$$E_0 = \sum_{i=1}^L \sum_{y=1}^{Y-1} \left\{ \gamma m_{it} + C_i(\mathbf{n}_y) m_{i,y} \left[ \log \frac{1}{1-c} - \frac{1}{2} (n_{i,y+1} + n_{i,y}) \log \frac{c}{1-c} \right] \right\} - \frac{1}{2} \sum_{i=1}^L (n_{i,1} + n_{i,Y}) \log \frac{c}{1-c}. \quad (12)$$

In deriving this, it is useful to note that the constraints on the configuration space of the model imply that  $(n_{i,y+1} - n_{i,y}) = C_i(\mathbf{n}_y) m_{i,y} (n_{i,y+1} - n_{i,y})$ ; on summing this equation over  $y$  the left hand side reduces to  $n_{i,Y} - n_{i,1}$ . One sees from (12) that the energy is symmetric under reversal of the time-like direction  $(n_{i,y}, m_{i,y}) \rightarrow (n_{i,Y+1-y}, m_{i,Y-y})$ . This symmetry is the same as time-reversal symmetry of the steady state of the dFA model, which follows from its detailed balance property.

Correspondence between the continuous-time FA model and this spin model requires that  $\gamma$  is large, by (10). This means that sites with  $m_i = 1$  are rare and also that for a given trajectory length  $\tau$ , it is necessary to use a very large lattice (because  $Y$  is large). However, numerical simulations are inefficient in this case. All qualitative features of this model depend weakly on  $\gamma$ , so we focus in the following on  $\gamma = 0$ .

Fig. 2(b) shows a representative configuration of the spin model with  $c = 0.38$  and  $\gamma = 0$ , generated by Monte Carlo sampling (see Appendix A). Since the mapping between the discrete-time FA model and the spin model is exact, this is also a representative trajectory of the dFA model. (A dynamical simulation of the dFA model would be a much simpler way to generate a similar trajectory, but this figure illustrates proof of principle.) The trajectory shown in Fig. 2(b) is also consistent with the behaviour of the FA model, see for example [29].

### 3.3. Free energy and large deviation formalism

The biased trajectory ensembles defined in (5) can be analysed by considering the  $2d$  spin model with a modified energy function. For any given  $2d$  spin configuration, the number of spin flips in the corresponding dFA model trajectory is

$$K = \sum_{i=1}^L \sum_{y=1}^{Y-1} [n_{iy}(1 - n_{i,y+1}) + (1 - n_{i,y})n_{i,y+1}]. \quad (13)$$

Hence the biased trajectory ensemble for the discrete-time FA model corresponds to a Boltzmann-Gibbs distribution of the  $2d$  spin model, where the energy  $E_0$  is replaced by

$$E_s = E_0 + sK = E_0 + s \sum_{i=1}^L \sum_{y=1}^{Y-1} [n_{iy} + n_{i,y+1} - 2n_{iy}n_{i,y+1}]. \quad (14)$$

For  $s > 0$ , this represents an additional ferromagnetic coupling for the spins, along the time-like bonds. The free energy difference (per site) between systems with energy  $E_s$



and  $E_0$  is a scaled cumulant generating function:

$$\hat{G}_{L,Y}(s) = \frac{1}{LY} \log \langle e^{-sK} \rangle_0, \quad (15)$$

where the angle brackets with subscript zero now indicate a Boltzmann average with energy  $E_0$ . This free energy  $\hat{G}$  is analogous to (3), but note the different normalisation: in the dynamical case we normalised by the trajectory length  $\tau$  (analogous to  $Y$  in this case); here we also normalised by  $L$ , to obtain a free energy per site. We use carets (hats) to distinguish functions for the  $2d$  spin model from their counterparts in the original FA model.

Also define  $\hat{\rho}_{L,Y}(k)$  as the probability density for  $k = K/(LY)$  [analogous to  $\rho_{L,\tau}(k)$  in Sec. 2.2]. The analogue of (7) is

$$\hat{\mathcal{G}}(s) = \lim_{L \rightarrow \infty} \lim_{Y \rightarrow \infty} \hat{G}_{L,Y}(s), \quad \hat{\mathcal{I}}(k) = \lim_{L \rightarrow \infty} \lim_{Y \rightarrow \infty} \frac{-1}{LY} \log \hat{\rho}_{L,Y}(k) \quad (16)$$

We identify  $\hat{\mathcal{G}}$  as the bulk free energy density. Note that there are no long-ranged terms in the energy function and the spin model has no other pathological features so we expect on general thermodynamic grounds that the order of limits should be irrelevant in these definitions, and that  $\hat{\mathcal{G}}(s)$  and  $\hat{\mathcal{I}}(k)$  should be related by Legendre transformation. We have not proven these results rigorously but all our results (and previous results for the FA model) are consistent with this hypothesis.

### 3.4. Periodic boundary conditions

In numerical studies of the dynamical phase transition that occurs in the FA model and other glassy models [14, 4, 15], finite-size scaling analyses are affected by the initial conditions in the trajectory averages of (3, 5). For the  $2d$  spin model considered here, the equilibrium ensemble of trajectories of the dFA model corresponds to taking free boundary conditions at  $y = 1$  and  $y = Y$ , as in (12, 13).

However, for the spin model, it is much more natural to consider a fully periodic system, instead of free boundary conditions. This also helps to reduce finite-size effects. To achieve this, we introduce an extra column of  $m$ -variables to the picture in Fig. 2(a), which are  $\mathbf{m}_Y = (m_{1,Y}, m_{2,Y}, \dots, m_{L,Y})$ . We also periodize (12, 13) by adding extra terms that couple the spins  $\mathbf{n}_1, \mathbf{n}_Y, \mathbf{m}_Y$ . In terms of the dFA model, this means that we consider the ensemble of trajectories that are periodic in time, see also [40]. Thermodynamic arguments indicate that the bulk free energy density should be  $\hat{\mathcal{G}}$  independent of boundary conditions. This result can be confirmed in this case because

$$\hat{G}_L(s) = \lim_{Y \rightarrow \infty} \hat{G}_{L,Y}(s) \quad (17)$$

can be obtained as the largest eigenvalue of a particular matrix [3, 4] (the tilted generator [20]), and this result is independent of whether one uses periodic or free boundary conditions at  $y = 1, Y$ .

All numerical results for the  $2d$  spin model use periodic boundary conditions, except where explicitly stated. Details of the simulation methods are given in Appendix A,

including some results with open boundaries. Note that some care is required with simulation of this spin model, because Monte Carlo moves that flip single  $n$  or  $m$  variables are not sufficient to allow access to all configurations of the system, if periodic boundary conditions are used. However, MC moves that additionally flip adjacent pairs of spins are sufficient to allow exploration of the whole configuration space, as discussed in [Appendix A](#).

#### 4. Phase transition in the $2d$ spin model: behaviour in finite systems

The dFA model has a dynamical phase transition, which corresponds to a thermodynamic phase transition in the  $2d$  spin model. These mean that the functions  $\hat{\mathcal{G}}(s), \hat{\mathcal{I}}(k)$  in (16) have the same behaviour as was illustrated in Fig. 1 for  $\mathcal{G}, \mathcal{I}$ . This can be proven by direct generalisation of the arguments of [4].

This Section presents numerical results for the thermodynamic transition in the  $2d$  spin model. As usual for numerical studies of phase transitions, the results are obtained in finite systems, so finite-size scaling analysis is required in order to interpret the results. Since these systems are anisotropic, this analysis requires some care with the ratio of  $Y/L$ , in the thermodynamic limit [34].

##### 4.1. Dynamical phase transition

To analyse the phase transition using data for finite systems we consider

$$k_{L,Y}(s) = \frac{1}{LY} \langle K \rangle_s = -\frac{d}{ds} \hat{\mathcal{G}}_{L,Y}(s), \quad (18)$$

which is the mean value of the order parameter, as well as the associated susceptibility

$$\chi_{L,Y}(s) = -\frac{d}{ds} k_{L,Y}(s), \quad (19)$$

which is proportional to the variance of  $K$ . The system has an active phase with large  $k$  and an inactive phase where most spins have  $n_i = 0$  and  $k$  is small. However, since configurations with  $\sum_i n_{i,y} = 0$  are forbidden, the inactive phase always includes at least one excitation line.

Fig. 3 shows results for a system with  $L = 32$  and  $Y = 512$ . As expected, the order parameter  $k_{L,Y}$  shows a crossover as  $s$  increases, with an associated peak in  $\chi_{L,Y}$ . Define the field  $s_{L,Y}^*$  to be the value of  $s$  that maximises  $\chi_{L,Y}(s)$ . Then the probability distribution

$$\hat{\rho}_*(k) = \hat{\rho}_{L,Y}(k|s_{L,Y}^*) \quad (20)$$

has a characteristic bimodal form in which the two peaks correspond to configurations from the active and inactive phases. The intermediate trough corresponds to configurations at phase coexistence. The configurations that are typical of the trough of  $\hat{\rho}_*$  depend on details of the system, including the aspect ratio  $Y/L$  and the surface tension between the phases. In this system, the fact that the inactive phase always contains at least one excitation line is also relevant. For the case considered in Fig. 3,

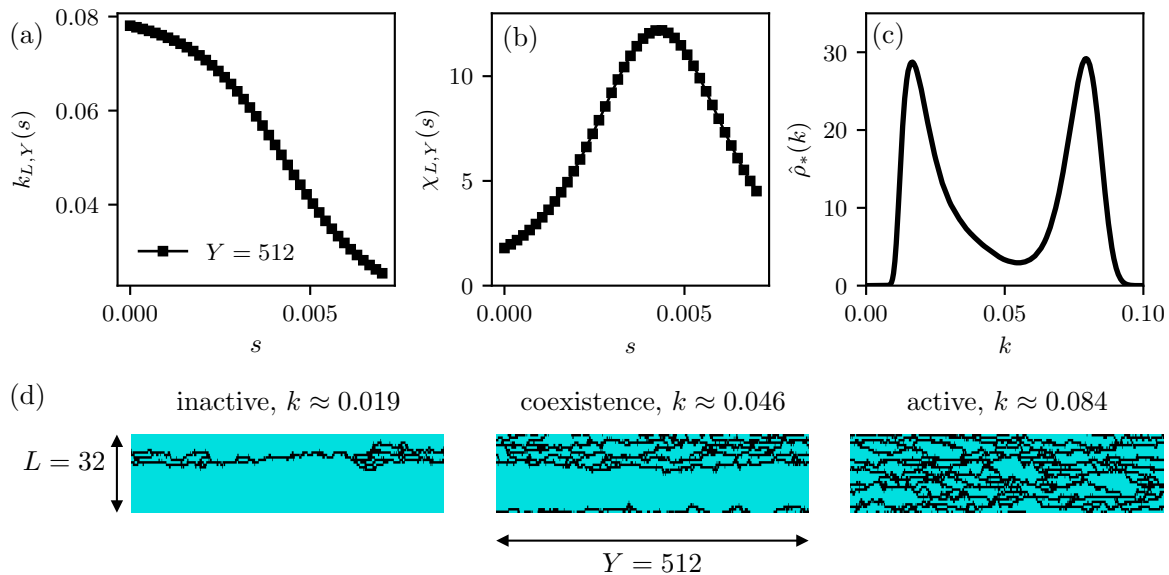


**Figure 3.** Results for the  $2d$  spin model  $L = 32$  and  $Y = 512$  and fully periodic boundary conditions. (a) Order parameter  $k(s)$ . (b) Susceptibility  $\chi(s)$ . (c) Histogram of the order parameter at  $s = s_{L,Y}^* = 0.0043$ . (d) Representative configurations taken from the two peaks of the histogram (active/inactive phases) and from the trough (phase coexistence). This is the expected behaviour in the regime  $L \sim Y$ .

one sees that phase coexistence corresponds to domains of active and inactive phases, with interfaces that lie parallel to the time-like axis.

#### 4.2. Finite-size scaling for $L \sim Y$

The data of Fig. 3 show the classical features of a first order phase transition. However, it is important to note that the behaviour of  $\hat{\rho}$  and the nature of the representative configurations depend on the aspect ratio  $Y/L$ . The behaviour of Fig. 3(c,d) is expected when  $L, Y$  are of the same order of magnitude, that is  $L \sim Y$  [34]. In this case, the two peaks of  $\hat{\rho}_*(k)$  appear at values  $k_a, k_i$  that are characteristic of the phases and depend weakly on  $L, Y$ . Hence the variance of  $k$  is of order unity, which corresponds to a peak in the susceptibility whose height diverges with the total size of the system:

$$\chi^* = \chi_{L,Y}(s_{L,Y}^*) \approx LY(k_a - k_i)^2/4. \quad (21)$$

Interfaces between active and inactive phases incur a free energy cost which depends on their orientation with respect to the lattice axes. Hence we define two surface tension parameters  $\Gamma_t, \Gamma_s$ , which are associated with interfaces that are parallel to the time-like and space-like axes respectively. (See also [22].) Since the interfaces in Fig. 3(d) are parallel to the time-like axis, we infer that the costs of the time and space directions satisfy  $Y\Gamma_t \ll L\Gamma_s$  so that  $\Gamma_t \ll (L/Y)\Gamma_s$ . The total length of the interface is  $2Y$ , so the peak-to-trough ratio of the distribution  $\hat{\rho}_{L,Y}^*$  scales as  $e^{-2Y\Gamma_t}$ , if one considers systems where the aspect ratio  $Y/L$  is held constant as  $Y \rightarrow \infty$ . With this scaling we emphasise

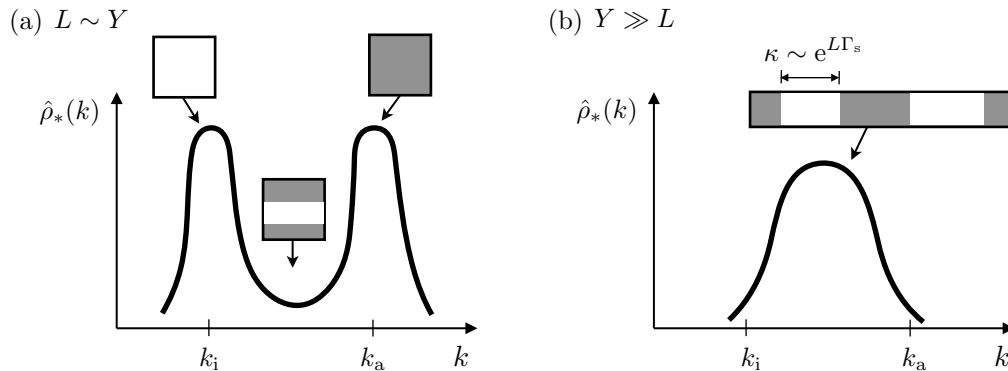


**Figure 4.** The finite-size scaling crossover of Privman and Fisher [34]. (a) For systems with  $Y \sim L$ , the classical picture of phase coexistence has a bimodal distribution of the order parameter. Representative configurations of the system are illustrated. The peaks correspond to the pure phases (illustrated in white and grey) and the trough corresponds to phase coexistence, shown here with domain walls parallel to the horizontal axis, as in Fig. 3. (b) For systems with  $Y \gg L$  the situation is different. The distribution of the order parameter is unimodal and typical configurations have many domains of both phases. The typical distance between domain walls scales as  $e^{L\Gamma_s}$ , see the text for a discussion.

that for values of  $k$  within the trough (that is,  $k_i < k < k_a$ ), one has

$$\lim_{L,Y \rightarrow \infty} \frac{-1}{LY} \log \hat{\rho}_{L,Y}(k|s_{L,Y}^*) = \lim_{L,Y \rightarrow \infty} (2\Gamma_s/L) = 0 \quad (22)$$

Hence from (16) one has  $\hat{\mathcal{I}}(k) = 0$  throughout this range, consistent with Fig. 1. The physical content of this result is that, in terms of cost, differences between configurations from the trough and the peaks of  $\hat{\rho}$  are localised at the interfaces. Since the interfaces occupy a vanishing fraction of the system, the difference in free energy between these configurations is subextensive, and the value of  $\frac{1}{LY} \log \hat{\rho}$  is the same. This is related to the Maxwell construction and the double tangent construction in thermodynamics [41].

### 4.3. Finite-size scaling and consequences for dynamical large deviations

So far, we analysed the behaviour of a finite system following the standard methods of thermodynamics. To make contact with the methods used for dynamical phase transitions, recall from (4) that the dynamical free energy is conventionally defined with a limit of large time  $\tau$  at fixed system size  $L$ . In the  $2d$  spin model, this corresponds to taking  $Y \rightarrow \infty$  at fixed  $L$ . The finite-size scaling behaviour for  $Y \gg L$  is quite different to that shown in Fig. 3, which applies for  $Y \sim L$ . This distinction was discussed by Privman and Fisher [34], who analysed thermodynamic phase transitions for different aspect ratios  $Y/L$ . This Section discusses the physical picture that follows from their analysis. Its consequences for the dynamical phase transition in the FA model will be discussed in Section 4.5.

From general thermodynamic arguments, the free energy  $\hat{\mathcal{G}}$  and its Legendre transform  $\hat{\mathcal{I}}$  in (16) are bulk quantities, independent of the its aspect ratio. In particular,

one should obtain the same result on interchanging the order of limits in (16), or on taking  $L, Y \rightarrow \infty$  together, with a fixed ratio  $Y/L$ . Moreover, Fig. 1 indicates that  $\hat{\mathcal{I}} = 0$  for  $k < \bar{k}$  in the FA model. Consistency of this picture with the dFA model requires that  $\frac{1}{LY} \log \hat{\rho}_{L,Y}(k|s_{L,Y}^*) \rightarrow 0$  in large systems, throughout the range  $0 < k < \bar{k}$  [see Eq. (22)]. For the situation where  $L \sim Y$  and the aspect ratio  $\alpha = Y/L$  is fixed in the thermodynamic limit, the expected behaviour is that

$$\log \hat{\rho}_{L,Y}(k|s_{L,Y}^*) \approx -L\mathcal{F}_\sim(k, \alpha, \Gamma_s, \Gamma_t), \quad k_i < k < k_a \quad (23)$$

where  $\mathcal{F}_\sim$  is the free energy cost for the interfaces associated with phase coexistence. The function  $\mathcal{F}_\sim$  also depends on the boundary conditions. The general form (23) is consistent with the behaviour of (22), which is relevant for the specific example in Fig. 3(d): in that case  $\mathcal{F}_\sim(k, \alpha, \Gamma_s, \Gamma_t) = 2\alpha\Gamma_t$ .

Note that (23) is an LDP with speed  $L$ , which describes the behaviour of the system at phase coexistence. Compared with the bulk result (16), it gives a more detailed description of the behaviour of  $\hat{\rho}_{L,Y}$ , for  $k_i < k < k_a$ . That is, the probability density  $\hat{\rho}$  obeys two LDPs: the ‘‘bulk’’ result (16) which has speed  $LY$  and the ‘‘interfacial’’ result (23). The bulk LDP has rate function zero throughout  $0 < k < \bar{k}$ , and this is independent of aspect ratio and boundary conditions. The interfacial LDP has a non-trivial rate function in this range of  $k$ ; it depends on both the aspect ratio and the boundary conditions.

To make contact with dynamical phase transitions, we now consider systems with  $Y \gg L$ , which are relevant for the dynamical LDP (2) and for (7). Fig. 4 shows the behaviour of  $\hat{\rho}_{L,Y}$  predicted by the theory of Privman and Fisher [34], and corresponding configurations of the system. For  $Y \gg L$ , phase coexistence is dominated by interfaces that are parallel to the space-like direction. The free-energy cost of a single interface is  $\Gamma_s L$  and these interfaces can appear anywhere along the time-like direction. It follows that for very large  $Y$ , the statistical properties of these domain walls are those of a one-dimensional ideal gas with density  $e^{-\Gamma_s L}$ . Hence their number follows a Poisson distribution with mean

$$\bar{n} \approx Y e^{-\Gamma_s L}. \quad (24)$$

Recalling (4) we are considering  $Y \rightarrow \infty$  at fixed  $L$ : to saturate this limit requires  $\bar{n} \gg 1$  or  $Y \gg e^{\Gamma_s L}$ . In this work, we use  $Y \gg L$  as a short-hand for the limit where  $Y \rightarrow \infty$  before any limit of large  $L$ . This corresponds to an extremely large aspect ratio  $Y/L$ . In thermodynamics, this regime is less often studied than the classical case  $Y \sim L$ , see however [34]. It is also harder to access by conventional MC simulations. However, it is the natural limit for the population dynamics (cloning) methods that are used to analyse dynamical large deviations [23, 24].

In this limit, the Poisson distribution for the number of domains means that the distribution  $\hat{\rho}^*(k)$  is peaked at  $(k_a + k_i)/2$ . The probability to have  $k \approx k_a$  or  $k \approx k_i$  can be estimated as the probability to have no domain walls at all, which for a Poisson distribution is simply  $e^{-\bar{n}}$ . In fact the statistics of the configurations shown in Fig. 4(b) are exactly those of a *one-dimensional* Ising model of size  $Y$  where the density of domain

walls is  $e^{-\Gamma_s L}$ . Equivalently one can identify these configurations with trajectories of a two-state Markov chain where each state corresponds to one of the phases, and the rate for transitions between the phases is  $e^{-\Gamma_s L}$ . In either case, the statistics of the activity are easily computed (see [Appendix B](#)) and one obtains

$$\log \hat{\rho}_{L,Y}(k|s_{L,Y}^*) \approx -Y \mathcal{F}_{\gg}(k), \quad k_i < k < k_a \quad (25)$$

with

$$\mathcal{F}_{\gg}(k) = e^{-\Gamma_s L} f\left(\frac{2(k - k_0)}{\Delta k}\right), \quad f(x) = 1 - \sqrt{1 - x^2}, \quad (26)$$

where  $k_0 = (k_a + k_i)/2$  is the average activity of the two phases and  $\Delta k = k_a - k_i$  is their difference. Eq. (25) is the analogue of (23) for systems with  $Y \gg L$ . We identify it as an LDP with speed  $Y$ . Again, this result gives extra detail on the behaviour of  $\hat{\rho}_{L,Y}$ , in the regime of phase coexistence. Consistent with the bulk LDP one has  $\frac{1}{LY} \log \rho \rightarrow 0$ . Note however that the LDP (25) is quite different from its counterpart (23) for  $L \sim Y$ . In particular, the rate function  $\mathcal{F}_{\gg}$  has a simple form that is convex, consistent with the unimodal distribution  $\hat{\rho}_*$  in Fig. 4(b). In contrast,  $\mathcal{F}_{\sim}$  in (23) is non-convex in general, consistent with the bimodal distributions in Figs. 3(c) and 4(a).

Noting that the LDP (25) applies to the distribution  $\hat{\rho}_{L,Y}(k|s_{L,Y}^*)$ , define  $s(k) = s_{L,Y}^* - \mathcal{F}'_{\gg}(k)$ , and note that the inverse of the function  $s(k)$  is  $k_{L,\infty}(s)$ . Hence

$$k_{L,\infty}(s) = k_0 - \frac{(s - s_{L,\infty}^*)(\Delta k)^2}{4\sqrt{(s - s_{L,\infty}^*)^2(\Delta k)^2 + (e^{-2\Gamma_s L}/4)}} \quad (27)$$

which describes the crossover between the phases as shown (for example) in Fig. 5(a). We will return to this result in Sec. 5, below. Note that (25) and (27) are generic for first-order dynamical phase transitions in two dimensions. The extension to higher dimensions is straightforward in the case where the system size along one dimension is much larger than the size along all others, in which case one should replace  $\Gamma_s L$  by  $\Gamma_s L^{d-1}$  for a suitably-defined surface tension parameter  $\Gamma_s$ . For dynamical phase transitions of mean-field systems, one expects a similar formula with an ‘‘interfacial cost’’  $\Gamma_s N$  where  $N$  is the system size, see [42]. In diffusive systems described by the Macroscopic Fluctuation Theory, see [43] for a discussion of similar phenomena.

#### 4.4. 2d spin model for $Y \gg L$

Fig. 5 illustrates the finite-size scaling crossover for the 2d spin model with  $L = 16$ . If  $Y$  is not too large then one observes a bimodal distribution of the order parameter, as in Fig. 3. However, one sees for larger  $Y$  a crossover to a unimodal form, consistent with Fig. 4. The representative configurations also show the crossover anticipated in Fig. 4, although the typical configurations have only one active and one inactive domain, even for the largest  $Y$  that we analysed. (To observe many domains would require even larger  $Y$ , which is numerically expensive.)

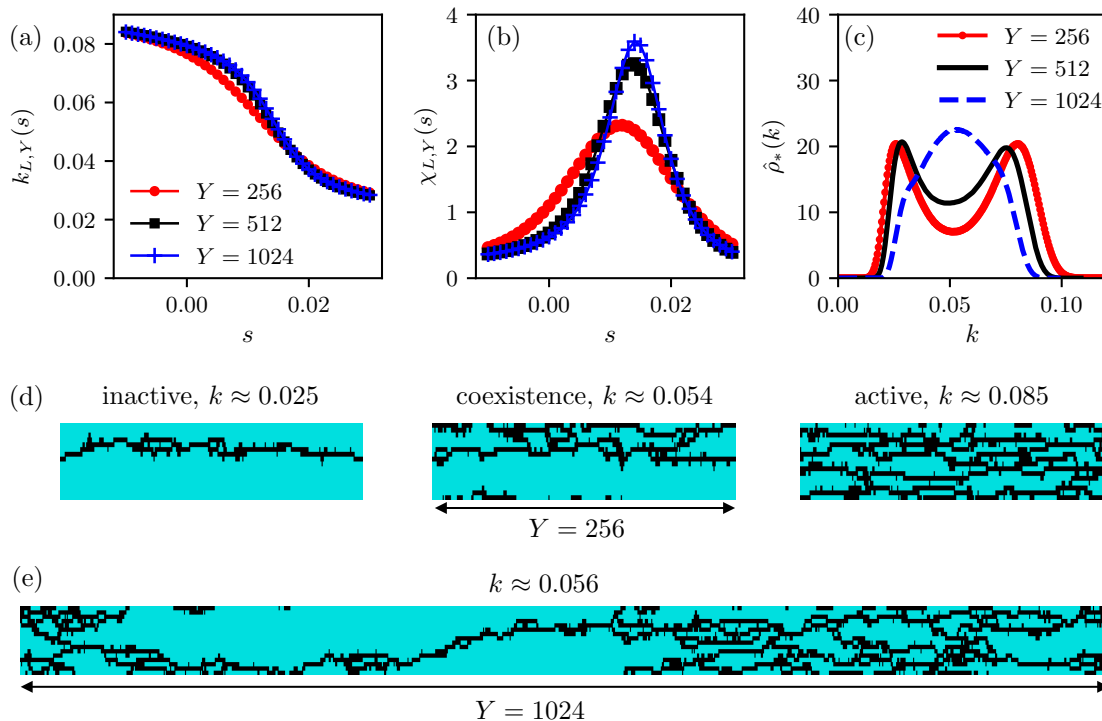


**Figure 5.** Results for  $L = 16$ . (a) Activity  $k(s)$  for different values of  $Y$ , as labelled, the data for  $Y = 512$  are very close to those for  $Y = 1024$ . (b) Susceptibility  $\chi(s)$ , the symbols and colours are the same as for panel (a). (c) Histograms of the activity at  $s = s^*$ . For smaller  $Y$  one sees a bimodal structure but for larger  $Y$  one sees a single peak, this is the Privman-Fisher crossover [34]. (d) Configurations at  $Y = 256$  showing behaviour that is representative of the two peaks in  $\rho_*$  (inactive/active phases), and of the intervening trough. (e) A configuration from  $Y = 1024$  that is representative of the peak of  $\rho_*$ , showing both phases coexisting in a single configuration. For even larger values of  $Y$ , typical trajectories would include multiple domains of each phase.

For large  $Y$ , one also sees that the order parameter  $k_{L,Y}(s)$  approaches a limiting form  $k_{L,\infty}(s)$ . To understand this, note that the thermodynamic analogue of the dynamical SCGF  $G_L(s)$  in (4) is

$$\hat{G}_{L,\infty}(s) = \lim_{Y \rightarrow \infty} \hat{G}_{L,Y}(s). \quad (28)$$

(To be precise, this corresponds to  $G_L(s)/L$ .) Following the same arguments as in the dynamical case, this limit exists and  $\hat{G}_{L,\infty}$  is strictly convex and analytic. Its derivative gives the limiting form of the order parameter  $k_{L,\infty}(s) = -G'_{L,\infty}(s)$ . From (27) one has also the corresponding susceptibility which is

$$\chi_{L,\infty}(s^*) \approx \frac{(\Delta k)^2}{4} e^{L\Gamma_s}. \quad (29)$$

This quantity diverges exponentially with  $L$ , in contrast to the power-law divergence of (21), which we recall was applicable for  $L \sim Y$ . This exponential scaling was observed for the (original) FA model in [27], where the connection to the work of Privman and Fisher was identified. Quantitative predictions for  $\Gamma_s$  were also obtained in that case, see Sec. 5.

#### 4.5. Connection to previous studies of dynamical phase transitions

We have used the  $2d$  spin model of Sec. 3.2 to illustrate the finite-size scaling crossover of Privman and Fisher [34]. Since the thermodynamics of this model are directly related to dynamical large deviations of the dFA model (and the FA model), we are now able to rationalise some of the previous work on finite-size scaling of dynamical phase transitions.

In particular, note that analysis of these phase transitions by transition path sampling [21] typically focusses on finite-size scaling with  $L \sim Y$  [15, 17]. For example the analysis of [15] assumes the scenario shown in Fig. 3, with a bimodal histogram of the order parameter. The associated peak-to-trough ratio increases with  $Y$  (or in that case  $\tau$ ), which was used in [15] as evidence for a first-order transition. Similar behaviour is seen in [17, 44]. In those cases one expects a power-law divergence of  $\chi_{L,Y}(s^*)$ .

On the other hand, analyses of dynamical phase transitions [23, 24] by cloning methods typically concentrate on the limit  $Y \gg L$ , as do analytical (and other) methods that estimate of the largest eigenvalue of a tilted generator [33]. In these cases the behaviour of  $\hat{\rho}_*$  close to its peak is described by (27), in which  $\mathcal{F}_{\gg}$  is a convex function. It follows that  $\hat{\rho}_*$  is unimodal, consistent with Figs. 4(b) and 5(c). We emphasise that this unimodal behaviour of  $\hat{\rho}_*$  is fully consistent with the existence of a phase transition, despite some of the arguments presented in [45]. In this case the susceptibility  $\chi_{L,\infty}(s^*)$  is expected to diverge exponentially with  $L$ , as observed in Ref. [27] for the FA model.

## 5. Interfacial model of phase coexistence

We have combined general theoretical arguments about first-order phase transitions with numerical calculations for the  $2d$  spin model. We now take an analytic approach to the dynamical phase transition in the FA model. Specifically, we expand on the work of [27], and we also correct some typographical errors in that work.‡ Our results yield a detailed understanding of the phase coexistence regime presented in the last section, and it gives a numerical value of the surface tension parameter  $\Gamma_s$  that determines the rate of exponential growth of the susceptibility.

### 5.1. Definition of interfacial model

We describe the phase transition in the FA model by a simplified interfacial model [31, 32], see also [27, 46]. We assume that the FA model at time  $t$  has a single large inactive domain where all spins have  $n_i = 0$ . Following [31, 32], we consider a continuous time Markov chain where the size of the *active* domain at time  $t$  is  $x_t \in \{1, 2, \dots, L\}$ , so the size of the inactive domain is  $L - x_t$ . The dynamical rule is that  $x$  follows an asymmetric random walk: it increases by a step of 1 with rate  $2q$  and decreases by a step of 1 with

‡ In particular, the main formula (9) of reference [27] is incorrect:  $F(c)$  in the left hand side should be replaced by  $F(c)/2$  and also the definition of  $F(c)$  should be  $(1/2) \log[1/(1-c)]$  instead of  $(1/2) \log[c/(1-c)]$ .



rate  $2p$ . If such a jump would lead to  $x > L$  or  $x < 1$  then it is rejected and  $x$  is unchanged. To reproduce the behaviour of the FA model requires

$$p = c(1 - c), \quad q = c. \quad (30)$$

Since  $p < q$  then the random walk is asymmetric and biased towards  $x = 1$  (which is the active phase). To parameterise the asymmetry of the walk we define

$$F = \frac{1}{2} \log \frac{q}{p} \quad (31)$$

which is positive but small in magnitude for our examples (of order  $c$ ). The natural microscopic time scale in the problem is  $(p + q)$ .

For a trajectory of the FA model where the size of the active domain is  $x(t)$ , one expects a dynamical activity

$$K(\tau) \approx \mathcal{K}(\tau) = \bar{k} \int_0^\tau x(t) dt \quad (32)$$

where the second equality defines  $\mathcal{K}(\tau)$ , which is the dynamical activity of a trajectory of the interfacial model. Eq. (32) assumes that behaviour within the active domain is close to the typical behaviour of the model, so the activity density there is close to  $\bar{k}$ . Note that  $\bar{k} = 4c^2(1 - c)$  in this model [27, 31, 32], different from the one introduced in previous sections.

For large  $L$ , it is convenient to replace the integer-valued domain size  $x$  by the fraction of the system that is covered by this domain, that is

$$y(t) = \frac{x(t)}{L} \quad (33)$$

In [27], this variable  $y(t)$  was denoted by  $\tilde{x}(t)$ . The analogue of the SCGF  $G_{L,\tau}(s)$  for this model is  $\Psi_{L,\tau}(sL)$  where

$$\Psi_{L,\tau}(\lambda) = \frac{1}{\tau} \log \left\langle e^{-\lambda \int_0^\tau y(t) dt} \right\rangle. \quad (34)$$

To the extent that the interfacial model captures the relevant physics in the FA model, we expect

$$G_{L,\tau}(s) \approx \Psi_{L,\tau}(sL). \quad (35)$$

The interfacial model does not capture all aspects of the FA model, in particular the fact that there are no fluctuations within the active phase is a coarse approximation. However, we will find that it is valid (at best) in regimes where the trajectories of the FA model contain large coexisting domains of active and inactive phases, with at most one large domain being present at any time  $t$ . This corresponds to values of  $s$  that are close to peaks of the susceptibility  $\chi$  that can be seen in Figs. 3, 5.

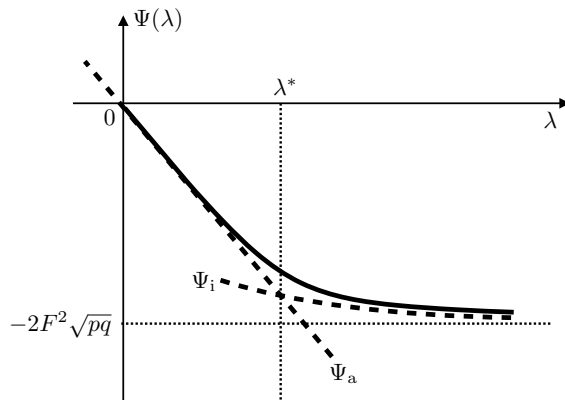


**Figure 6.** Sketch of the SCGF  $\Psi_L(\lambda)$ , shown as a solid line. The dashed lines show the behaviour of the active and inactive phases. The active phase has  $\Psi_a \approx -\lambda\bar{k}$  with a correction at order  $1/L$  (the mean activity  $\mathcal{K}/(L\tau)$  of this phase is  $\bar{k}$ ). Also  $\Psi_i \approx -2\sqrt{pq}F^2$ , with a finite-size correction of order  $L^{-2/3}$ , see (60). The dashed lines cross at  $\lambda = \lambda^* \approx 2F^2\sqrt{pq}/\bar{k}$ . The SCGF  $\Psi$  deviates from  $\max(\Psi_a, \Psi_i)$  by a quantity that scales as  $e^{-L\Gamma}$ , where the constant  $\Gamma$  is given by (70). This means that the curvature  $\Psi''(\lambda)$  is exponentially large for  $\lambda \approx \lambda^*$ .

## 5.2. Large deviation analysis

We now consider large deviations of the interfacial model in the limit of large  $\tau$ , so we define

$$\Psi_L(\lambda) = \lim_{\tau \rightarrow \infty} \Psi_{L,\tau}(\lambda) \quad (36)$$

analogous to  $G_L(s)$  in the FA model, see (4). The following analysis applies for  $\lambda \geq 0$  and we also assume that  $F \ll 1$ , which simplifies the analysis. The results are summarised in Fig. 6. For large- $L$  this result is consistent with Fig. 1(b), but we emphasise again that the behaviour for finite  $L$  is specific to a system where the limit of large time  $\tau$  is taken before any limit of large  $L$ . Note also that  $\Psi_L$  is decreasing and convex, so we have for  $\lambda \geq 0$  that

$$-\lambda\bar{k} \leq \Psi_L(\lambda) \leq 0. \quad (37)$$

*5.2.1. Eigenvalue problem in continuous space* The SCGF can be obtained by solving an eigenproblem, based on the master equation for the dynamics [4]. Within the bulk of the system ( $y \neq \frac{1}{L}, 1$ ) one has

$$\Psi_L(\lambda)P_L(y) = 2p[P_L(y + \frac{1}{L}) - P_L(y)] + 2q[P_L(y - \frac{1}{L}) - P_L(y)] - \lambda y\bar{k}P_L(y) \quad (38)$$

where the eigenvector  $P_L$  is a (discrete) probability distribution for  $y$ . In the following we sometimes omit the subscripts  $L$ , for compactness of notation. At the boundaries one has

$$\begin{aligned} \Psi P(\frac{1}{L}) &= 2pP(\frac{2}{L}) - 2qP(\frac{1}{L}) - \lambda\bar{k}/L \\ \Psi P(1) &= 2qP(\frac{L-1}{L}) - 2pP(1) - \lambda\bar{k}. \end{aligned} \quad (39)$$

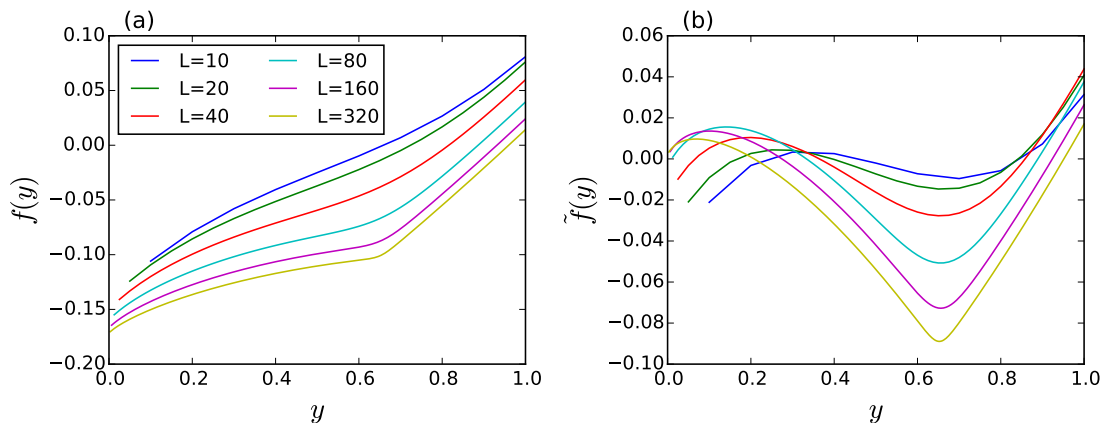


**Figure 7.** The rate functions  $f(y)$  and  $\tilde{f}(y)$  at coexistence, evaluated for finite values of  $L$  by diagonalizing the eigenvalue problem (38). The value of  $c$  is set to 0.3. The value of  $\lambda$  is tuned to the special value that maximizes the curvature  $\Psi''(\lambda)$  for each  $L$ . The figures show that  $\tilde{f}(y)$  has two maxima at coexistence, whereas  $f(y)$  does not.

Eqs. (38, 39) define an eigenvalue problem for an  $L \times L$  matrix, which is easily solved numerically. Here we adopt an analytical approach, which gives insight into the limit of large  $L$ . Our analysis also requires that  $F \ll 1$ .

In the large- $L$  limit, we find that the eigenvector  $P$  takes the form

$$P(y) = \exp[Lf(y)], \quad (40)$$

where  $f$  is of order unity. For example, in the absence of any bias,  $f(y) = 2Fy$  and the the distribution of  $y$  is exponentially increasing, with a maximum at  $y = 1$ . (This is the active phase.)

In general, the eigenfunction  $P$  gives the distribution of the size of the active domain, evaluated at the final time  $\tau$ . The meaning of (40) is that this size obeys an LDP with speed  $L$  and rate function  $-f(y)$ . It is convenient to define also  $Q(y) = P(y)e^{-LFy}$ , in which case  $Q(y)^2$  is a (non-normalised) probability distribution for the domain size  $y_t$ , where  $t$  is in the “bulk” of the trajectory (*i.e.* far from initial and final times). In the notation of [27], we thus have  $P_{\text{ave}}(y) \propto Q(y)^2$  and  $P_{\text{end}}(y) = P(y)$ . One sees that  $P_{\text{ave}}$  also satisfies an LDP with speed  $L$ , that is

$$Q(y)^2 = \exp[L\tilde{f}(y)], \quad \tilde{f}(y) = 2[f(y) - yF]. \quad (41)$$

At the dynamical phase transition,  $\tilde{f}(y)$  presents two maxima as shown in Fig. 7 for finite  $L$ , and the corresponding values of  $y$  are the sizes of the active domain in the coexisting phases. We emphasise however that the LDPs (40, 41) for  $y_t$  are distinct from the LDP for the time-integrated quantity  $\mathcal{K}$  that is our main interest here.

The passage from the discrete-space problem to a continuum one is discussed in Appendix C. We define

$$\mu = \left( \frac{\lambda \bar{k}}{2\sqrt{pq}} \right)^{1/3}, \quad \psi_L = \frac{\Psi_L(\lambda)}{2\sqrt{pq}} + F^2. \quad (42)$$

Note that  $\mu \geq 0$  is known (it depends only on the parameters of the model) but  $\psi_L$  is unknown (it depends on the eigenvalue  $\Psi_L$ ). We recognise  $\psi_L$  as the difference between the solid line and the horizontal dotted line in Fig. 6. The function  $Q$  satisfies the self-adjoint eigenvalue equation (C.11) which reduces to

$$\frac{1}{L^2}Q_L''(y) - \mu^3 y Q_L(y) = \psi_L Q_L(y) \quad (43)$$

This equation is to be solved subject to the boundary conditions (C.12) which are

$$\frac{Q'(0)}{LQ(0)} = \gamma_0 = F + (\psi - F^2) + O(F^3), \quad \frac{Q'(1)}{LQ(1)} = \gamma_1 = F + (\psi + \mu^3 - F^2) + O(F^3). \quad (44)$$

This equation defines  $\gamma_0, \gamma_1$ . (The quantities in round brackets are  $O(F^2)$ , we retain them for later convenience. Note that ignoring terms at  $O(F^3)$  can sometimes lead to artificial solutions to the eigenproblem with  $\psi > 0$ , see Appendix C.3.)

Since the coefficient of  $Q''$  in (43) is small, one may obtain approximate solutions to the eigenproblem. This is equivalent to a WKB-like saddle-point analysis method. Here we take a different route, using that (43) can be solved exactly using Airy functions.

*5.2.2. Solution of the eigenvalue problem* The Airy functions are solutions of the Airy equation  $f''(x) - xf(x) = 0$ , and are denoted by  $\text{Ai}(x)$  and  $\text{Bi}(x)$ . For negative  $x$ , these functions oscillate around zero. For positive  $x$ ,  $\text{Ai}$  is a decreasing function and  $\text{Bi}$  is increasing. For large positive  $x$  they behave as

$$\begin{aligned} \text{Ai}(x) &\simeq \exp\left(-\frac{2}{3}x^{3/2}\right) \frac{1}{2\sqrt{\pi}x^{1/4}} [1 + O(x^{-3/2})], \\ \text{Bi}(x) &\simeq \exp\left(\frac{2}{3}x^{3/2}\right) \frac{1}{2\sqrt{\pi}x^{1/4}} [1 + O(x^{-3/2})]. \end{aligned} \quad (45)$$

Note in particular that  $\text{Bi}(x)$  grows super-exponentially when its argument is large.

By changing variables in (43), its solution can be seen to be

$$Q_L(y) = \hat{a}_L \mathcal{A}_L(y) + \hat{b}_L \mathcal{B}_L(y) \quad (46)$$

where  $\hat{a}_L, \hat{b}_L$  are coefficients with a normalisation condition  $\hat{a}_L + \hat{b}_L = 1$  and

$$\begin{aligned} \mathcal{A}_L(y) &= \text{Ai}\left[L^{2/3}\left(\mu y + \frac{\psi_L}{\mu^2}\right)\right], \\ \mathcal{B}_L(y) &= \frac{1}{\text{Bi}\left(L^{2/3}\left(\mu + \frac{\psi_L}{\mu^2}\right)\right)} \text{Bi}\left[L^{2/3}\left(\mu y + \frac{\psi_L}{\mu^2}\right)\right]. \end{aligned} \quad (47)$$

Note that  $\mathcal{B}$  is normalised such that  $\mathcal{B}_L(1) = 1$ . From (37, 42) we have

$$-\mu^3 \leq (\psi - F^2) \leq 0 \quad (48)$$

which implies in particular that  $\psi + \mu^3$  is (strictly) positive, and the asymptotic expansions of (45) are relevant. To keep track of exponential factors in the large- $L$  limit, it is useful to define

$$\epsilon_L = \exp\left[-\frac{2}{3}L\left(\mu + \frac{\psi_L}{\mu^2}\right)^{3/2}\right]. \quad (49)$$

which is exponentially small when  $L$  is large. With this choice one sees that  $\mathcal{A}_L(1)$  and  $\mathcal{B}_L(0)$  are both of order  $\epsilon_L \cdot L^{-1/6}$ .

The physical interpretation of (46) is that  $\mathcal{A}_L$  and  $\mathcal{B}_L$  have peaks near 0 and 1 respectively and represent contributions to the eigenfunction from the two phases. The weights  $\hat{a}$ ,  $\hat{b}$  and the unknown quantity  $\psi_L$  must now be determined from the boundary condition (44). This requires that

$$\frac{\hat{a}_L}{\hat{b}_L} = \frac{\mathcal{B}'(0) - L\gamma_0\mathcal{B}(0)}{L\gamma_0\mathcal{A}(0) - \mathcal{A}'(0)} = \frac{\mathcal{B}'(1) - L\gamma_1\mathcal{B}(1)}{L\gamma_1\mathcal{A}(1) - \mathcal{A}'(1)} \quad (50)$$

Recall that  $\mathcal{B}(0)$  and its derivative are exponentially small when  $L$  is large, and similarly for  $\mathcal{A}(1)$ . To compensate these exponential factors, define

$$\eta_L = [\mathcal{B}'(0) - L\gamma_0\mathcal{B}(0)]/\epsilon_L, \quad \xi_L = [L\gamma_1\mathcal{A}(1) - \mathcal{A}'(1)]/\epsilon_L. \quad (51)$$

To simplify notation define also

$$V_L = L\gamma_0\mathcal{A}(0) - \mathcal{A}'(0), \quad W_L = \mathcal{B}'(1) - L\gamma_1\mathcal{B}(1). \quad (52)$$

Then the second equality in (50) is

$$\frac{\epsilon_L\eta_L}{V_L} = \frac{W_L}{\epsilon_L\xi_L}. \quad (53)$$

The objects  $\eta_L, V_L, W_L, \xi_L$  do not depend on  $\hat{a}_L$  or  $\hat{b}_L$  but they do depend on  $\mu, F$  (which are parameters of the model) and on  $\psi_L$ . The presence of the small quantity  $\epsilon_L$  in these equations allows the behaviour of  $\psi_L$  to be determined.

Observe that none of  $\eta_L, V_L, W_L, \xi_L$  grow exponentially with  $L$ . Hence there are three possibilities in (53). The first is that  $W_L$  is proportional to  $\epsilon_L^2$  for large  $L$ , but  $V_L$  is well-behaved (in the sense that it does not have an exponential dependence on  $L$ ). In this case  $\hat{a}_L/\hat{b}_L$  is proportional to  $\epsilon_L$  so the eigenfunction  $Q$  is dominated by a peak at  $y \approx 1$ . This will correspond to the active phase. The second possibility is that  $V_L$  is proportional to  $\epsilon_L^2$  for large  $L$ , but  $W_L$  is well-behaved. In this case  $\hat{b}_L/\hat{a}_L$  is proportional to  $\epsilon_L$  so the eigenfunction  $Q$  is dominated by a peak at  $y \approx 0$ . This will be the inactive phase. The third possibility is that both  $V_L$  and  $W_L$  are proportional to  $\epsilon_L$  so that  $\hat{b}_L/\hat{a}_L$  is well-behaved. This corresponds to phase coexistence.

We consider the three cases in turn. Note there is no symmetry between the two phases in this problem.

*5.2.3. Active phase* The active phase corresponds to exponentially small values of  $W_L$  which means that

$$\mathcal{B}'(1) = L\gamma_1\mathcal{B}(1) + O(\epsilon_L^2) \quad (54)$$

Within the active phase, we ignore the exponentially small correction. For large  $x$  the Airy function has  $\text{Bi}'(x)/\text{Bi}(x) \approx x^{1/2}$  from which one obtains

$$\mu^3 + \psi_L \approx \gamma_1^2 \quad (55)$$

Recalling that  $F$  is small, we have from (44) that  $\gamma_1^2 = F^2 + O(F^3)$  which yields  $\psi_L - F^2 \approx \mu^3 + O(F^3)$  or equivalently

$$\Psi_L \approx \Psi_a = -\lambda \bar{k} \quad (56)$$

which was the result anticipated in Fig. 6 for the active phase. (The second equality is the definition of  $\Psi_a$ , the first equality is approximate and holds up to corrections at  $O(F^3)$ .)

*5.2.4. Inactive phase* For the inactive phase then  $V_L$  is small which means that

$$L\gamma_0 \mathcal{A}(0) = \mathcal{A}'(0) + O(\epsilon_L^2) \quad (57)$$

As before we drop the term at order  $\epsilon_L^2$  and obtain

$$L\gamma_0 \text{Ai}(L^{2/3}\psi_L/\mu^2) = \mu L^{2/3} \text{Ai}'(L^{2/3}\psi_L/\mu^2) \quad (58)$$

Recall that  $\gamma_0 = F + O(F^2)$  is positive. The derivative  $\text{Ai}'(x)$  is negative for  $x > 0$  so  $\psi_L < 0$ . However,  $\text{Ai}'(x)$  oscillates for  $x < \alpha_0$  where  $\alpha_0 \approx -2.3$  is the zero of  $\text{Ai}$  closest to  $x = 0$ . It follows that for large  $L$ , the argument of the Airy function must converge to  $\alpha_0$  and one sees that

$$\psi_L \approx -|\alpha_0| \mu^2 L^{-2/3} \quad (59)$$

Hence

$$\Psi_L(\lambda) \approx \Psi_i(\lambda) = -2\sqrt{pq}F^2 + O(L^{-2/3}) \quad (60)$$

as anticipated in Fig. 6. This behaviour was discussed in [31, 32]. The non-integer power in the finite-size correction reflects the fact that  $\mathcal{A}_L(y)$  tends to zero as  $y \rightarrow 0$  but it has a maximum at a value of order  $L^{-2/3}$ , indicating that the typical value of  $x = yL$  is large but subextensive, of order  $L^{1/3}$ . That is, the inactive phase contains a single domain where the activity is non-zero: this domain covers a large number of sites, but not enough to constitute a finite fraction of the system [31, 32].

*5.2.5. Phase coexistence* From the analysis of the two phases and recalling Fig. 6, we see that the crossover between the phases takes place when  $\Psi_a \approx \Psi_i$ , which corresponds to  $\mu = \mu_L^*$  with

$$\mu_L^* \approx F^{2/3} \quad (61)$$

or equivalently

$$\lambda^* \bar{k} \approx 2\sqrt{pq}F^2 \quad (62)$$

consistent with Fig. 6. Note also that  $\psi_L^* \approx 0$  by (59). Within each individual phase, one of the factors  $V_L$  and  $W_L$  in (53) is exponentially small, such that (50) is satisfied. Close to  $\lambda^*$ , both these quantities are small. We analyse this situation in a general setting with minimal assumptions on the functions  $V_L, W_L$ . The method is quite generic for first-order phase transitions: it amounts to constructing an eigenfunction  $Q_L$  from

two basis functions (here  $\mathcal{A}, \mathcal{B}$ ) which have exponentially small overlap. The aim is to compute the behaviour of the eigenvalue  $\psi$  as the parameter  $\mu$  is increased.

Consider (54, 57), and drop the correction terms at  $O(\epsilon_L^2)$ . These equations can be solved simultaneously for  $(\mu, \psi)$ . We denote the solution by  $(\mu_L^*, \psi_L^*)$ , which corresponds to the point where  $\Psi_a = \Psi_i$  in Fig. 6. Note that if we substitute the values  $(\mu_L^*, \psi_L^*)$  then  $V_L = 0 = W_L$  exactly but (53) is manifestly not satisfied in this case. In fact, the true value of  $\psi_L$  at this value of  $\mu$  differs from  $\psi_L^*$  by a correction at  $O(\epsilon_L)$ , recall again Fig. 6.

We are not able to estimate  $(\mu_L^*, \psi_L^*)$  with exponential accuracy, but we are able to make an expansion about  $\mu = \mu_L^*$  that captures the small deviation of  $\psi_L$  from  $\psi_L^*$ . To this end, write

$$(\mu_L, \psi_L) = (\mu_L^* + \delta\mu, \psi_L^* + \delta\psi) \quad (63)$$

and substitute in (53). Using  $\partial_\mu$  to indicate a partial derivative with respect to  $\mu$ , and similarly  $\partial_\psi$ , one obtains

$$\epsilon_L^2 \eta_L \xi_L = [(\delta\mu)\partial_\mu W_L + (\delta\psi)\partial_\psi W_L] \cdot [(\delta\mu)\partial_\mu V_L + (\delta\psi)\partial_\psi V_L] \quad (64)$$

where all derivatives are evaluated at  $(\mu^*, \psi^*)$ . It is not necessary to estimate these derivatives directly, instead we rewrite the equation in a generic form by introducing new constants  $X_1, X_2, Z$  (dependent on the model parameters and on  $\mu_L^*, \psi_L^*$ ), such that

$$(\delta\psi + X_1\delta\mu) \cdot (\delta\psi + X_2\delta\mu) - \epsilon_L^2 Z^2 (X_2 - X_1)^2 = 0 \quad (65)$$

Consistency of this approach requires  $X_1 \neq X_2$  and  $Z^2 > 0$  but this is always the case in practice. We take  $X_2 > X_1$  without loss of generality. Solving for  $\delta\psi$ , we obtain

$$\delta\psi = \pm \frac{1}{2}(Y - X)\sqrt{(\delta\mu)^2 + (\epsilon_L Z)^2} - \frac{X + Y}{2}\delta\mu \quad (66)$$

We take the + sign for the square root because  $\psi$  is known to be a convex function of  $\mu$ , see also below. Using (42) one has for small  $\delta\mu$  that  $\lambda - \lambda_L^* \approx C\delta\mu$  with  $C = \frac{6\sqrt{pq}}{k}(\mu_L^*)^2$ . Hence

$$\frac{1}{2\sqrt{pq}}\Psi_L(\lambda) = \psi_L^* - F^2 + \frac{X_2 - X_1}{C}\sqrt{(\lambda - \lambda_L^*)^2 + (\epsilon_L Z C)^2} - \frac{X_1 + X_2}{2C}(\lambda - \lambda_L^*) \quad (67)$$

which is the finite-size scaling form for  $\Psi$ , valid for small  $\lambda - \lambda_L^*$ . Differentiating with respect to  $\lambda$  gives the behaviour of the order parameter near the transition:

$$k_L(\lambda) = -\Psi'_L(\lambda) = \frac{\sqrt{pq}}{C} \left[ (X_2 + X_1) - \frac{(X_2 - X_1)(\lambda - \lambda_L^*)}{\sqrt{(\lambda - \lambda_L^*)^2 + (\epsilon_L Z C)^2}} \right]. \quad (68)$$

This function is of the same form as (27), showing that the general analysis of Sec. 4.3 is consistent with the specific calculation of this section. It shows a crossover at  $\lambda = \lambda_L^*$ , from a value  $2\sqrt{pq}X_2/C$  (at small  $\lambda$ ) to  $2\sqrt{pq}X_1/C$  (at large  $\lambda$ ). Comparing with (27) one identifies these quantities as the activities of the two phases. The width of the crossover is  $1/(CZ\epsilon_L)$ , which diverges exponentially with the system size when  $L$  is

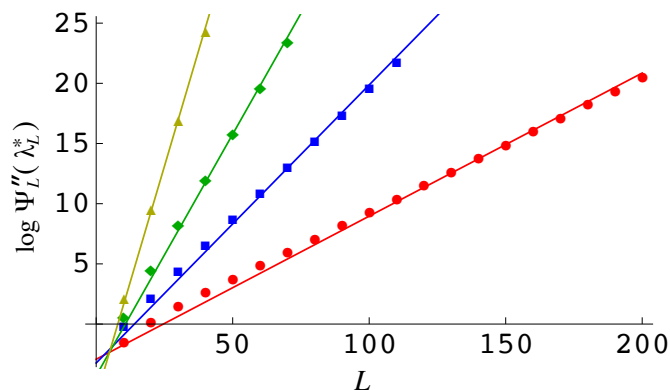


**Figure 8.** The logarithm of the second derivative of SCGF at the transition point  $\lambda_L^*$  as a function of the system size  $L$ :  $\Psi_L''(\lambda_L^*)$ . We numerically diagonalize the matrix of the largest eigenvalue problem (38), evaluate the second derivative of the largest eigenvalue  $\Psi_L(\lambda)$ , and find the maximum of the second derivative  $\Psi_L''(\lambda)$ :  $\max_\lambda \Psi_L''(\lambda) \equiv \Psi_L''(\lambda_L^*)$ . Red circles, blue squared, green diamonds, yellow triangles correspond to  $c = 0.3, c = 0.5, c = 0.7, c = 0.9$ , respectively. We also plot the analytical prediction Eq. (70) as solid lines:  $\log \Psi_L''(\lambda_L^*) = (2F/3)L + \text{const}$ .

large. From (27) we identify this with  $e^{\Gamma_s L}/(\Delta k)^2$  where  $\Delta k$  is the difference in activity between the phases. The maximal susceptibility is

$$\Psi_L''(\lambda_L^*) = \frac{X_2 - X_1}{2ZC^2} \cdot \frac{1}{\epsilon_L} \quad (69)$$

which indeed diverges exponentially with  $L$ , as anticipated in Fig. 6. The rate of this exponential divergence is fixed by the scaling of  $\epsilon_L$ . Using (61) and that  $\psi_L^* \approx 0$  one obtains from (49) exponential divergence of the susceptibility:

$$\Psi_L''(\lambda_L^*) \sim e^{\Gamma_s L}, \quad \Gamma_s = 2F/3 + O(F^2). \quad (70)$$

The exponential scaling is consistent with the general arguments of Sec. 4.4 and we identify  $\Gamma_s$  as the surface tension. In Fig. 8, we compare (70) with numerical results for  $\Psi_L''(\lambda_L^*)$ , showing good agreement. The analysis of this section also predicts the eigenfunction  $Q$  which gives the probability distribution of  $y_t$ , at the coexistence point. Note that the prediction (70) for  $\Gamma_s$  is accurate up to corrections at  $O(F^2)$ . A more accurate numerical prediction is also available if one accounts for higher-order terms when solving (55), see [27] for details.

We conclude that the interfacial model predicts the scaling of the order parameter near the dynamical phase transition to be (68) and it also makes quantitative predictions including (62, 70). These have been shown [27, 33] to agree very well with numerical computations on the FA model. This confirms the prediction (35) that the interfacial model can capture the behaviour of the FA model close to its dynamical phase transition, including the relevant phase behaviour.



## 6. Conclusion

We have analysed the dynamical phase transition that occurs in the FA model, by two methods. In Sec. 4, we invoked a correspondence between FA model trajectories and configurations of the  $2d$  spin model, in order to relate dynamical properties of FA model to thermodynamic properties of this spin model. We used the analysis of Privman and Fisher [34] to rationalise the finite-size scaling properties of this spin model, and we emphasised the differences in behaviour for systems with  $Y \sim L$  and  $Y \gg L$ . In the dynamical case, the first case corresponds to trajectories where the time  $\tau$  and the system size  $L$  are both large; the second case is relevant on taking the limit  $\tau \rightarrow \infty$  before any limit of large  $L$ , as is often the case in studies of dynamical LDPs.

In this second case, we explained how the distribution of the order parameter at phase coexistence takes a unimodal form for large  $\tau$ , and the associated susceptibility diverges exponentially fast with  $L$ . This is in contrast to the case  $Y \sim L$  which is more conventionally analysed in thermodynamics, where the distribution is bimodal and the susceptibility diverges as a power law. For  $Y \gg L$ , we also derived the general predictions (25, 27) for the finite-size scaling behaviour close to phase coexistence, based on the physical picture of Fig. 4(b). See also [39].

In Section 5 we performed a specific analysis of the behaviour close to dynamical phase coexistence in the FA model, using the interfacial model discussed in [27], see also [31, 32]. The result is consistent with the general formulae (25, 27) but it also gives more detailed predictions, including the value of the surface tension parameter  $\Gamma_s$ , and the forms of the eigenfunctions  $Q$ , which specify the probability distribution for the instantaneous size of the large inactive domain in the system.

The FA model is simple enough to enable this analysis, but the phase transitions that we have analysed exhibit the full phenomenology of first-order phase transitions in finite-dimensional systems. We hope that these results will be useful in guiding the future analysis of other dynamical phase transitions and their finite-size scaling properties.

## Acknowledgments

VL is supported by the ERC Starting Grant No. 680275 MALIG, the ANR-18-CE30-0028-01 Grant LABS and the ANR-15-CE40-0020-03 Grant LSD.

## Appendix A. MC simulation of the $2d$ spin model

To analyse thermodynamic properties of the  $2d$  spin model, we use MC simulations. Given a configuration  $\mathcal{C}$  we propose a new configuration  $\mathcal{C}'$ . The new configuration is accepted with probability  $\min(1, e^{E_s(\mathcal{C}) - E_s(\mathcal{C}')} )$  where the energy  $E_s$  is given by (14), generalised to periodic boundaries if applicable. Otherwise the old configuration is retained.

In the simplest MC algorithm, one chooses either a spin  $n_{i,y}$  or  $m_{i,y}$  at random and one proposes a new configuration by flipping this spin. However, for systems with periodic boundaries, the constraints on the  $n$  and  $m$  variables means that updating the configuration in this way does not allow access to every possible configuration of the system. As an example, consider the following configuration of a periodic system with  $(L, Y) = (4, 5)$ , where X and . indicate sites with  $n_i = 1, 0$  respectively and  $-$  indicates a bond with  $m_i = 1$ .

```
X X X X X
X- . .-X X
X X- . .-X
X X X X X
```

It can be checked that there is no sequence of single-spin flips that connect this configuration to the state where  $n_{i,y} = 1$  for all  $i, y$ . The essential problem is that there are two spins in the third column with  $n_{i,y} = 0$  (indicated by .), but neither of these spins is able to flip, because of the constraint that  $m_{i\pm 1} = 0$  if  $m_i = 1$ .

The solution is that in addition to proposed moves where only one spin is flipped, we also propose occasionally moves where two spins  $n_{i,y}$  and  $n_{i,y+1}$  are both flipped simultaneously. We claim that this gives an MC method that samples the full configuration space of the model. For small systems we have verified explicitly every allowed configuration can be reached from every other configuration.

With this MC algorithm, the system explores its configuration space slowly, but computations are feasible. For calculations in large systems close to phase transitions (Figs. 3, 5), we use two methods. For  $L = 16$  we performed long simulations with  $s \approx s^*$ , so that the system visits both phases many times during the course of a single MC run. A histogram of  $K$  is accumulated in this run, and  $k(s)$  and  $\chi(s)$  are obtained as weighted average with respect to that histogram. For  $L = 32$  we performed parallel tempering simulations in which multiple replicas of the system are simulated at different values of  $s$ , with all values of  $s$  being close to  $s^*$ . The histograms from the data at different  $s$  are combined using the unbinned weighted histogram analysis method [47], which yields an estimate for the distribution of  $K$ . This distribution is then used to derive  $k(s)$  and  $\chi(s)$  by weighted averages.

Finally, to demonstrate the effect of different boundary conditions, Fig. A1 shows data for a very small system ( $L = 8$ ). Taking  $Y \rightarrow \infty$  at fixed  $L$ , one expects convergence of  $k(s)$  and  $\chi(s)$  to smooth limiting forms at large  $Y$ . The figure shows that  $Y = 128$  is already very close to convergence of this limit in a system with periodic boundaries. By contrast, the system which corresponds exactly to the equilibrium trajectory ensemble of the dFA model has a much stronger finite-size effect, in that larger  $Y$  is required to see convergence to the large- $Y$  limit. The reason is that the regions close to  $y = 1$  and  $y = Y$  are biased by the boundary conditions towards the active phase, which hinders characterisation of the phase coexistence regime. See also [17].

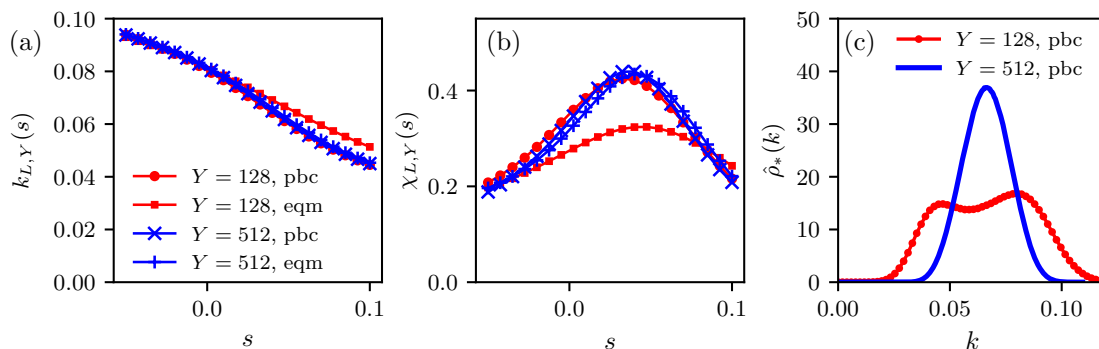


**Figure A1.** Data for the  $2d$  spin model at  $L = 8$ . We show results for systems with periodic boundaries (pbc), and for systems with energy (14), which includes boundary terms that are chosen to recover the equilibrium trajectory ensemble of the dFA model (eqm). (a) Order parameter  $k_{L,Y}(s)$ . (b) Susceptibility  $\chi_{L,Y}(s)$ , the colours and symbols are the same as in panel (a). (c) Finite size scaling of  $\hat{\rho}_*$ , only for the periodic case. Even if the function  $k_{L,Y}(s)$  has saturated to its large- $Y$  limit, the shape of this distribution still depends on  $Y$ .

## Appendix B. Simple model for multi-domain phase coexistence

We describe the fluctuations in configurations such as those sketched in Fig. 4(b). These are representative configurations of the  $2d$  spin model at  $s = s^*$ . They can be modelled by considering a  $1d$  Ising model with periodic boundaries whose typical domain size is  $\kappa \approx e^{\Gamma s L} \gg 1$ . The same results may alternatively be obtained by considering large deviations of a two-state Markov chain. Working at temperature  $T = 1$  we introduce a magnetic field  $h \ll 1$  so the free energy of the Ising model can be obtained by standard methods as  $\lambda(h) = -\frac{1}{Y} \log \text{Tr}(M_h^Y)$  where the transfer matrix is

$$M_h = \begin{pmatrix} 1 + h & \kappa^{-1} \\ \kappa^{-1} & 1 - h \end{pmatrix}. \quad (\text{B.1})$$

where we work at leading order in  $h, \kappa^{-1}$ . For large  $Y$  then  $\lambda(h)$  is given by (the negative of) the largest eigenvalue of this matrix so  $\lambda(h) = -1 - \sqrt{h^2 + \kappa^{-2}}$ . The SCGF for the total magnetisation of the  $1d$  Ising model (in this limit) is  $g(h) = \lambda(0) - \lambda(h)$  so

$$g(h) = \sqrt{h^2 + \kappa^{-2}} - \kappa^{-1}. \quad (\text{B.2})$$

The derivative of this function gives the mean magnetisation as a function of the field

$$m(h) = g'(h) = \frac{h}{\sqrt{h^2 + \kappa^{-2}}}. \quad (\text{B.3})$$

The total magnetisation obeys an LDP whose speed is the number of sites in this  $1d$  Ising model, which is  $Y$ . The rate function for this total magnetisation is  $J(m) = \sup_h (hm - g(h))$  which yields

$$J(m) = \kappa^{-1}(1 - \sqrt{1 - m^2}), \quad -1 < m < 1. \quad (\text{B.4})$$

This rate function describes the fluctuations of the amount of each phase, assuming that the domain walls in the configuration of Fig. 4(b) are a dilute ideal gas. Neglecting

fluctuations within the phases, we identify the (intensive) activity of a configuration as  $k = k_0 + (m\Delta k/2)$  where  $k_0$  is the average activity of the two phases, and  $\Delta k$  is the difference between their activities. Hence (B.4) yields (25, 26).

## Appendix C. Discrete and continuous versions of the interfacial model

### Appendix C.1. Continuum limit

We show how the interfacial model (defined on a discrete lattice) can be analysed by considering a continuous probability distribution for  $y$ . Starting from (38) and using (40) we obtain (after Taylor expansion of  $f$  with  $L \gg 1$ ):

$$\Psi + \lambda y \bar{k} = 2p \left( e^{f'(y)} [1 + f''(y)/(2L)] - 1 \right) + 2q \left( e^{-f'(y)} [1 + f''(y)/(2L)] - 1 \right). \quad (\text{C.1})$$

So far this result only requires that  $L$  is large. In order to obtain an eigenvalue problem for the continuous function  $P$ , we now assume additionally that  $|f'(y)| \ll 1$  everywhere, which leads to

$$\Psi + \lambda y \bar{k} = (2p - 2q)f'(y) + (p + q)[f'(y)^2 + f''(y)/L]. \quad (\text{C.2})$$

We will see that this corresponds physically to approximating the binomial distribution of the discrete random walk by a Gaussian distribution, as in a diffusion process. When considering the typical behaviour of the system, this approximation is exact for large  $L$ , but large deviations can be sensitive to the full distribution of hop sizes. For the problem considered here, we make an approximation when expanding over  $f'$  but the resulting theory still gives semi-quantitative predictions (see Fig. 8 and Fig. C1). Identifying

$$L f'(y) = \frac{d}{dy} \log P(y) = \frac{P'(y)}{P(y)} \quad (\text{C.3})$$

and

$$L f''(y) = \frac{d^2}{dy^2} \log P(y) = \frac{P''(y)}{P(y)} - \frac{P'(y)^2}{P(y)^2}, \quad (\text{C.4})$$

one obtains

$$(\Psi + \lambda y)P(y) = \frac{2(p - q)}{L} P'(y) + \frac{p + q}{L^2} P''(y) \quad (\text{C.5})$$

which is an eigenvalue equation for the continuous function  $P$ . The boundary conditions (39) are treated similarly, in order to obtain constraints on  $f'(0)$  and  $f'(1)$ . However, the point about which the Taylor expansion is performed is optimised to minimise errors associated with the expansion at small  $f'$ . To this end note that

$$\frac{P((n+1)/L) - P(n/L)}{P((n+1)/L) + P(n/L)} = \frac{e^{f'} - 1}{e^{f'} + 1} = \tanh(f'/2) = \frac{f'}{2} + O(f')^3 \quad (\text{C.6})$$

where we use the shorthand  $f' = f'(\frac{2n+1}{2L})$ , for compactness of notation. The correction on the right hand side is  $O(f')^3$ : other representations of the derivative are possible but

would have corrections at  $O(f')^2$  which is less accurate. The boundary conditions (39) are

$$\frac{P(2/L) - P(1/L)}{P(2/L) + P(1/L)} = c_0, \quad \frac{P(1) - P((L-1)/L)}{P(1) + P((L-1)/L)} = c_1 \quad (\text{C.7})$$

with  $c_0 = \frac{2q-2p+\Psi_L}{2q+2p+\Psi_L}$  and  $c_1 = \frac{2q-2p-\Psi_L-\lambda\bar{k}}{2q+2p+\Psi_L+\lambda\bar{k}}$ . Hence (C.6) provides values for  $f'(\frac{3}{2L})$  and  $f'(\frac{2L-1}{2L})$  which we identify (at large  $L$ ) with  $f'(0)$  and  $f'(1)$ . Using again (C.3) yields

$$\frac{P'(0)}{P(0)} = 2c_0L, \quad \frac{P'(1)}{P(1)} = 2c_1L. \quad (\text{C.8})$$

### Appendix C.2. Simplification for small $F$

Note that in addition to a large- $L$  limit, we have assumed that  $f'(y) \ll 1$ . For  $\lambda = 0$  it is easily verified that the exact eigenvector of the discrete problem has  $f'(y) = 2F = \log(q/p)$  so self-consistency requires that this parameter be small. Physically, this requires that the hop rate for the asymmetric random walk  $x_t$  is much larger than its drift, that is  $(p-q)/(p+q) \ll 1$ .

In this case it is consistent to identify  $(p-q) = 2\sqrt{pq} \sinh F \approx 2F\sqrt{pq}$  and  $(p+q) = 2\sqrt{pq} \cosh F \approx (2+F^2)\sqrt{pq}$ . Using this result in (C.5) yields (at leading order)

$$\frac{1}{2\sqrt{pq}}(\Psi + \lambda\bar{k}y)P(y) = \frac{2F}{L}P'(y) + \frac{1}{L^2}P''(y) \quad (\text{C.9})$$

and the associated boundary conditions are

$$\frac{P'_L(0)}{P_L(0)} = 2L \cdot \frac{F\sqrt{pq} + (\Psi_L/4)}{\sqrt{pq} + (\Psi_L/4)}, \quad \frac{P'_L(1)}{P_L(1)} = 2L \cdot \frac{F\sqrt{pq} - (\Psi_L + \lambda\bar{k})/4}{\sqrt{pq} + (\Psi_L + \lambda\bar{k})/4}. \quad (\text{C.10})$$

To see that the small- $F$  approximation is self-consistent, note that for  $\lambda = 0$  one has  $\Psi_L = 0$  and this recovers  $P(y) = e^{2LFy}$ , which is the exact result in the discrete case.

To transform the eigenvalue problem to a self-adjoint form we define  $Q(y) = P(y)e^{-LFy}$ , which yields

$$\frac{1}{2\sqrt{pq}}(\Psi + \lambda\bar{k}y)Q(y) = \frac{1}{L^2}Q''(y) - F^2Q(y). \quad (\text{C.11})$$

As  $L \rightarrow \infty$ , one sees (consistent with Fig. 6) that both  $\Psi$  and  $\lambda\bar{k}$  will be  $O(F^2)$ . Hence the boundary conditions for  $Q$  can be derived as

$$\frac{Q'(0)}{Q(0)} = L \left( F + \frac{\Psi}{2\sqrt{pq}} + O(F^3) \right), \quad \frac{Q'(1)}{Q(1)} = L \left( F - \frac{\Psi + \lambda\bar{k}}{2\sqrt{pq}} + O(F^3) \right). \quad (\text{C.12})$$

### Appendix C.3. Numerical demonstrations

We use numerical results to compare solutions of the continuous eigenvalue problem (43) and the original discrete eigenvalue problem (38), in order to demonstrate the validity of the continuous limit.

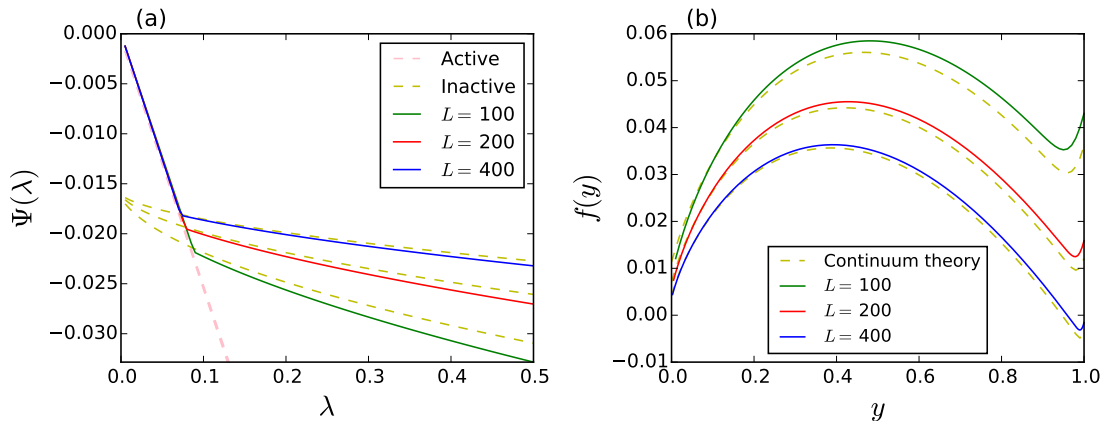


**Figure C1.** (a) The SCGF  $\Psi(\lambda)$  obtained from the discrete eigenvalue problem (38) (solid lines) and continuous eigenvalue problem (43) (dashed lines). The value of  $c$  is 0.3. The active and inactive solutions for the continuous problem are obtained following the procedure detailed in the main text. (b) The behaviour of  $f(y) = (1/L) \log P_L(y)$  in the inactive phase, for  $(c, \lambda) = (0.3, 0.2)$ . We show good agreement between solutions of the discrete problem [Eq. (38), solid lines] and those obtained by solving the continuous problem [Eq. (43), dashed lines].

For the discrete problem, we numerically diagonalize the matrix on the right-hand side of (38) and obtain  $\Psi(\lambda)$  as the largest eigenvalue and  $P_L(y)$  as the associated eigenvector. For the continuous problem, we use the general solution (46) of the eigenvalue problem (43, 44), where the parameter  $\hat{b}_L$  is set to 1 without loss of generality and the parameter  $\hat{a}_L$  is determined using one of the boundary conditions (43) and (44). The other boundary condition is used to determine the value of  $\psi$  (as the largest solution that satisfies the boundary condition), from which we obtain  $\Psi(\lambda)$ . There are two technical remarks related to the boundary conditions. First, depending on which boundary condition is used to determine  $\hat{a}_L$ , the obtained solution  $\psi$  changes: if the boundary condition for  $y = 0$  (or  $y = 1$ ) is used to determine  $\hat{a}_L$ , we obtain the solution of  $\psi$  that corresponds to the active (or inactive) phase. This means that, irrespective of the value of  $\lambda$ , we can construct both active and inactive solutions by exploiting this property (see Fig. C1, the solution with larger  $\psi$  gives the free energy and the other solution corresponds to a metastable state). Second, if we ignore the  $O(F^3)$  terms in the boundary conditions (43) and (44), we may obtain an artificial solution in some cases (with  $\psi > 0$ ). To avoid this problem, we use the full expression of the boundary conditions (*i.e.*, the expression that includes  $O(F^3)$  terms<sup>§</sup>). Alternatively, this problem can be avoided by retaining the truncated boundary conditions and restricting to solutions with  $\psi < 0$ .

Fig. C1(a) shows  $\Psi(\lambda)$  for these discrete and continuous problems. Fig. C1(b) shows  $f(y) = (1/L) \log P_L(y)$  for a representative state point in the inactive phase. For

<sup>§</sup> The complete boundary condition that includes  $O(F^3)$  can be derived from (C.10), it is also provided in Supplementary Material of Ref. [27].

large- $L$ , there is good agreement between the solutions of the discrete and continuous eigenvalue problems, as expected. Recall that we derived the continuous eigenvalue equation (43) from the discrete eigenvalue equation (38) by assuming that the slope of  $f(y)$  is small. Our numerical observation shows that  $f(y)$  has a zero slope for  $y \sim 0.5$ , and keeps a relatively small slope around  $y \sim 0.5$  (except for around  $y = 0$  or  $y = 1$ ), which is consistent with this small- $f'(y)$  assumption. Fig. C1 shows results for  $c = 0.3$ ; qualitatively similar results were also obtained in the range of  $c$  between  $c = 0.1$  and  $c = 0.7$  (not shown).

To understand the physical interpretation of the results in Fig. C1(b), recall from Sec. 5.2.1 that the maximum of  $f$  corresponds to the most likely value of  $y_\tau$ , where  $\tau$  is the final time of the trajectory. The different behaviours of  $P_L$  and  $Q_L$  [defined in Eqs. (40, 41)] mean that the most likely value of  $y_\tau$  differs from the typical values of  $y_t$  in the bulk of the trajectory (far from initial and final times). The average values of  $y_t$  in the bulk of these trajectories are (0.117, 0.0771, 0.0506) for  $L = (100, 200, 400)$ ; these small values are consistent with the system being in the inactive phase.

## Bibliography

- [1] Frank den Hollander. *Large deviations*. American Mathematical Society Providence, RI 2000.
- [2] Bernard Derrida. [Non-equilibrium steady states: fluctuations and large deviations of the density and of the current](#). *J. Stat. Mech.* **2007**, P07023 (2007).
- [3] V. Lecomte, C. Appert-Rolland, and F. van Wijland. [Thermodynamic formalism for systems with Markov dynamics](#). *J. Stat. Phys.* **127**, 51 (2007).
- [4] Juan P Garrahan, Robert L Jack, Vivien Lecomte, Estelle Pitard, Kristina van Duijvendijk, and Frédéric van Wijland. [First-order dynamical phase transition in models of glasses: an approach based on ensembles of histories](#). *J. Phys. A* **42**, 075007 (2009).
- [5] H. Touchette. [The large deviation approach to statistical mechanics](#). *Phys. Rep.* **478**, 1 (2009).
- [6] Lorenzo Bertini, Alberto De Sole, Davide Gabrielli, Giovanni Jona-Lasinio, and Claudio Landim. [Macroscopic fluctuation theory](#). *Rev. Mod. Phys.* **87**, 593 (2015).
- [7] Joel L. Lebowitz and Herbert Spohn. [A Gallavotti-Cohen-type symmetry in the large deviation functional for stochastic dynamics](#). *J. Stat. Phys.* **95**, 333 (1999).
- [8] Todd R Gingrich, Jordan M Horowitz, Nikolay Perunov, and Jeremy L. England. [Dissipation Bounds All Steady-State Current Fluctuations](#). *Phys. Rev. Lett.* **116**, 120601 (2016).
- [9] Takahiro Nemoto, Étienne Fodor, Michael E. Cates, Robert L. Jack, and Julien Tailleur. [Optimizing active work: Dynamical phase transitions, collective motion, and jamming](#). *Phys. Rev. E* **99**, 022605 (2019).
- [10] T. Bodineau and B. Derrida. [Current Fluctuations in Nonequilibrium Diffusive Systems: An Additivity Principle](#). *Phys. Rev. Lett.* **92**, 180601 (2004).
- [11] A. Baule and R. M. L. Evans. [Invariant Quantities in Shear Flow](#). *Phys. Rev. Lett.* **101**, 240601 (2008).
- [12] Pablo I. Hurtado, Carlos P. Espigares, Jesús J. del Pozo, and Pedro L. Garrido. [Thermodynamics of Currents in Nonequilibrium Diffusive Systems: Theory and Simulation](#). *J. Stat. Phys.* **154**, 214 (2014).
- [13] Chloe Ya Gao and David T. Limmer. [Nonlinear transport coefficients from large deviation functions](#). *The Journal of Chemical Physics* **151**, 014101 (2019).
- [14] J. P. Garrahan, R. L. Jack, V. Lecomte, E. Pitard, K. van Duijvendijk, and F. van Wijland. [Dynamical First-Order Phase Transition in Kinetically Constrained Models of Glasses](#). *Phys. Rev. Lett.* **98**, 195702 (2007).

- [15] L. O. Hedges, R. L. Jack, J. P. Garrahan, and D. Chandler. [Dynamic Order-Disorder in Atomistic Models of Structural Glass Formers](#). *Science* **323**, 1309 (2009).
- [16] R. L. Jack and P. Sollich. [Large Deviations and Ensembles of Trajectories in Stochastic Models](#). *Prog. Theor. Phys. Supp.* **184**, 304 (2010).
- [17] Yael S. Elmatad, Robert L. Jack, David Chandler, and Juan P. Garrahan. [Finite-temperature critical point of a glass transition](#). *Proc. Natl. Acad. Sci. USA* **107**, 12793 (2010).
- [18] D Ruelle. [Thermodynamic Formalism](#), Addison & Wesley. *Reading, MA* (1978).
- [19] M. Merolle, J. P. Garrahan, and D. Chandler. [Space-time thermodynamics of the glass transition](#). *Proc. Natl. Acad. Sci. USA* **102**, 10837 (2005).
- [20] Raphaël Chétrite and Hugo Touchette. [Nonequilibrium Markov processes conditioned on large deviations](#). *Ann. Henri Poincaré* **16**, 2005 (2015).
- [21] P. G. Bolhuis, D. Chandler, C. Dellago, and P. L. Geissler. [Transition path sampling: Throwing ropes over rough mountain passes, in the dark](#). *Ann. Rev. Phys. Chem.* **53**, 291 (2002).
- [22] Robert L. Jack, Juan P. Garrahan, and David Chandler. [Space-time thermodynamics and subsystem observables in a kinetically constrained model of glassy materials](#). *J. Chem. Phys.* **125**, 184509 (2006).
- [23] Cristian Giardinà, Jorge Kurchan, and Luca Peliti. [Direct Evaluation of Large-Deviation Functions](#). *Phys. Rev. Lett.* **96**, 120603 (2006).
- [24] Vivien Lecomte and Julien Tailleur. [A numerical approach to large deviations in continuous time](#). *J. Stat. Mech.* **2007**, P03004 (2007).
- [25] R. L. Jack and P. Sollich. [Effective interactions and large deviations in stochastic processes](#). *Eur. Phys. J.: Spec. Topics* **224**, 2351 (2015).
- [26] Raphaël Chétrite and Hugo Touchette. [Variational and optimal control representations of conditioned and driven processes](#). *J. Stat. Mech.* **2015**, P12001 (2015).
- [27] Takahiro Nemoto, Robert L. Jack, and Vivien Lecomte. [Finite-Size Scaling of a First-Order Dynamical Phase Transition: Adaptive Population Dynamics and an Effective Model](#). *Phys. Rev. Lett.* **118**, 115702 (2017).
- [28] Glenn H. Fredrickson and Hans C. Andersen. [Kinetic Ising model of the glass transition](#). *Phys. Rev. Lett.* **53**, 1244 (1984).
- [29] J. P. Garrahan and D. Chandler. [Geometrical explanation and scaling of dynamical heterogeneities in glass forming systems](#). *Phys. Rev. Lett.* **89**, 035704 (2002).
- [30] David Chandler and Juan P. Garrahan. [Dynamics on the Way to Forming Glass: Bubbles in Space-Time](#). *Ann. Rev. Phys. Chem.* **61**, 191 (2010).
- [31] T. Bodineau and C. Toninelli. [Activity Phase Transition for Constrained Dynamics](#). *Commun. Math. Phys.* **311**, 357 (2012).
- [32] Thierry Bodineau, Vivien Lecomte, and Cristina Toninelli. [Finite Size Scaling of the Dynamical Free-Energy in a Kinetically Constrained Model](#). *J. Stat. Phys.* **147**, 1 (2012).
- [33] Mari Carmen Bañuls and Juan P. Garrahan. [Using Matrix Product States to Study the Dynamical Large Deviations of Kinetically Constrained Models](#). *Phys. Rev. Lett.* **123**, 200601 (2019).
- [34] Vladimir Privman and Michael E. Fisher. [Finite-size effects at first-order transitions](#). *J. Stat. Phys.* **33**, 385 (1983).
- [35] Christian Borgs and Roman Kotecký. [A rigorous theory of finite-size scaling at first-order phase transitions](#). *Journal of Statistical Physics* **61**, 79 (1990).
- [36] Christian Borgs and Roman Kotecký. [Finite-size effects at asymmetric first-order phase transitions](#). *Phys. Rev. Lett.* **68**, 1734 (1992).
- [37] M. D. Donsker and S. R. S. Varadhan. [Asymptotic evaluation of certain markov process expectations for large time, I](#). *Comm. Pure Appl. Math.* **28**, 1 (1975).
- [38] Raphaël Chétrite and Hugo Touchette. [Nonequilibrium Microcanonical and Canonical Ensembles and Their Equivalence](#). *Phys. Rev. Lett.* **111**, 120601 (2013).
- [39] Robert L. Jack. [Ergodicity and large deviations in physical systems with stochastic dynamics](#). arXiv:1910.09883.



- [40] G Biroli and J Kurchan. Metastable states in glassy systems. *Phys. Rev. E* **64**, 016101 (2001).
- [41] Kerson Huang. *Introduction to Statistical Physics*. CRC press Boca Raton, FA 2nd edition 2010.
- [42] Takahiro Nemoto, Vivien Lecomte, Shin ichi Sasa, and Frédéric van Wijland. [Finite-size effects in a mean-field kinetically constrained model: dynamical glassiness and quantum criticality](#). *J. Stat. Mech.* **2014**, P10001 (2014).
- [43] Yongjoo Baek, Yariv Kafri, and Vivien Lecomte. [Dynamical phase transitions in the current distribution of driven diffusive channels](#). *Journal of Physics A: Mathematical and Theoretical* **51**, 105001 (2018).
- [44] Thomas Speck and David Chandler. [Constrained dynamics of localized excitations causes a non-equilibrium phase transition in an atomistic model of glass formers](#). *J. Chem. Phys.* **136**, 184509 (2012).
- [45] Stephen Whitelam. [Large deviations in the presence of cooperativity and slow dynamics](#). *Phys. Rev. E* **97**, 062109 (2018).
- [46] Jakub Dolezal and Robert L. Jack. *J. Stat. Mech.*, in press. arXiv:1906.07043.
- [47] Zhiqiang Tan, Emilio Gallicchio, Mauro Lapelosa, and Ronald M. Levy. [Theory of binless multi-state free energy estimation with applications to protein-ligand binding](#). *J. Chem. Phys.* **136**, 144102 (2012).